SIAM J. Applied Dynamical Systems
Vol. 13, No. 4, pp. 1489–1516

Traveling Waves in a One-Dimensional Elastic Continuum Model of Cell Layer Migration with Stretch-Dependent Proliferation*

Tracy L. Stepien† and David Swigon‡

Abstract. Collective cell migration plays a substantial role in maintaining the cohesion of epithelial cell layers and in wound healing. A number of mathematical models of this process have been developed, all of which reduce to essentially a reaction-diffusion equation with diffusion and proliferation terms that depend on material assumptions about the cell layer. In this paper we extend a one-dimensional mathematical model of cell layer migration of Mi et al. [*Biophys. J.*, 93 (2007), pp. 3745–3752] to incorporate stretch-dependent proliferation, and show that this formulation reduces to a generalized Stefan problem for the density of the layer. We solve numerically the resulting partial differential equation system using an adaptive finite difference method and show that the solutions converge to self-similar or traveling wave solutions. We analyze self-similar solutions for cases with no proliferation, and necessary and sufficient conditions for existence and uniqueness of traveling solutions for a wide range of material assumptions about the cell layer.

Key words. cell migration, wound healing, mathematical modeling, elastic continuum, free boundary problem, traveling wave solutions

AMS subject classifications. 92C05, 35R35, 35C06, 35C07

DOI. 10.1137/130941407

1. Introduction.

Cells of epithelial layers and other tissues have the ability to repair gaps in the layer by migration into the damaged area. This migration proceeds in a coordinated fashion so that no new gaps are formed in the cell layer, a process called collective cell migration (Friedl and Gilmour [9]; Rørth [18]). Migration is directed by polarization of cells and physical and biochemical interactions between cells. Epithelial cells are mechanically linked to each other via adherens junction and desmosomal proteins, integrins, and tight and gap junctions (Ilina and Friedl [13]).

The closure speed of any gap in the cell layer is affected by the surrounding cells and environment. For example, cell proliferation does not contribute to closure; rather, damaged cells are replaced in part to restore the original cell layer density (Farooqui and Fenteany [7]). Also, growth factor signals lead to directed migration of leader cells but do not affect the migration and coordination of follower cells (Vitorino and Meyer [27]). In terms of the environment, adhesion between cells and the substrate as well as the stiffness of the substrate affect the velocity of cells closing gaps in the layer (Palecek et al. [17], Ghibaudo et al. [12]). Furthermore, cells throughout the layer actively contribute to the movement of the layer in

*Received by the editors October 16, 2013; accepted for publication (in revised form) by B. Sandstede July 18, 2014; published electronically October 30, 2014.
http://www.siam.org/journals/siads/13-4/94140.html
†Department of Mathematics, University of Pittsburgh, Pittsburgh, PA 15260. Current address: School of Mathematical and Statistical Sciences, Arizona State University, Tempe, AZ 85287 (tstepien@asu.edu). This author's work was supported by NSF award EMSW21-RTG 0739261 and by an Andrew Mellon Predoctoral Fellowship.
‡Department of Mathematics, University of Pittsburgh, Pittsburgh, PA 15260 (swigon@pitt.edu).

the direction toward the gap, partly evidenced by traction forces applied by migrating cells on the substrate arising several rows behind the moving edge, and the velocity within a cell layer was found to be inversely proportional to the distance from the wound edge (Farooqui and Fenteany [7], Trepat et al. [26]).

Many existing continuum models of cell migration in wound healing are based on reaction-diffusion equations in which the moving edge of a cell layer is represented as a traveling wave of cell concentration; see, for example, Sherratt and Murray [20, 21] and Maini, McElwain, and Leavesley [14]. Some models involve a free boundary problem, which accounts for the influence of physiological effects on wound closure; Gaffney et al. [11] developed a free boundary problem for a system of reaction-diffusion equations for cell density and chemical stimulus for corneal wound healing, and then Chen and Friedman [4] analyzed that model as well as another free boundary problem that applied to tumor growth [5]. Xue, Friedman, and Sen [28] developed a model with a free boundary problem for ischemic dermal wounds that was used to predict how ischemic conditions may impair wound closure. Models of cell migration based on reaction-diffusion equations do not account for essential mechanical forces, so constitutive assumptions cannot be validated to describe the material properties of epithelial cell layers.

In this paper we extend the model framework of Mi et al. [15], while maintaining their basic assumption that the one-dimensional cell layer is represented by an elastic continuum capable of deformation, motion, and material growth. The motion of the cell layer is assumed to be driven by the cells at the moving edge through the formation of lamellipodia (Sheetz, Felsenfeld, and Galbraith [19]). Interior cells are tightly connected to the cells at the boundary, and tight junctions prevent separation between neighboring cells (Anand et al. [1]). The interior cells have also been observed forming lamellipodia, but their direction is not as highly correlated as for the cells at the edge. The cell layer stretches because tension is applied by the edge cells, and the motion of the cells in the interior is slowed down by the adhesion between cells and the substrate. Compared to Mi et al. [15], we generalize the formulation to an arbitrary elasticity function governing the stretchability of the layer and an arbitrary proliferation function governing the growth and degradation of the layer. We show that for broad classes of elasticity and proliferation functions the motion of a semi-infinite layer in the present model converges to a stable traveling wave with a unique velocity. We develop both the material (Lagrangian) and the spatial (Eulerian) formulations of the problem and find that the material formulation leads to a simpler algorithm for numerical solutions, while the analysis of traveling waves is easier in the spatial formulation.

The outline of the paper is as follows: in section 2 we formulate the governing equations of the model in the material formulation; in section 3 we give numerical solutions of the material formulation of the problem on a finite domain, which suggests the presence of traveling waves; and in section 4 we analyze a similarity solution under scaling in the spatial formulation for a case with no proliferation. Finally, in section 5 we prove the existence and uniqueness of traveling wave solutions in the spatial formulation for cases with proliferation and use numerical methods to show that traveling waves are stable as long as they do not contain local maxima or minima of cell density.

2. Model formulation.

In this section we follow the material (Lagrangian) formulation of the model first introduced by Mi et al. [15]. The main interactions governing the motion of

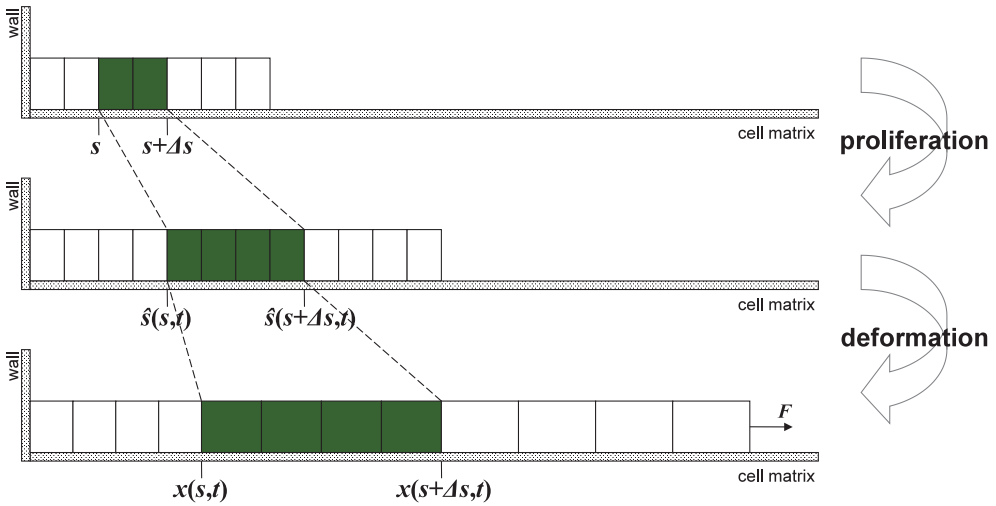

Figure 1. *Schematic representation of the cell layer as a one-dimensional continuum: (top) initial state; (middle) hypothetical state at time t, accounting for proliferation but not deformation; (bottom) true configuration of the layer at time t.*

the cell layer are the force of the lamellipodia, adhesion of the cell layer to the substrate, and elasticity of the cell layer. Elasticity of the substrate is neglected since the original motivation for the model comes from in vitro scratch wound assay experiments which studied intestinal epithelial cells on glass coverslips. This model differs from published viscoelastic continuum models of epithelial sheets, such as that of Tranquillo and Murray [25], which consider elastic forces and traction forces arising from the actin filament network between the cells and the substrate that attaches to the cells.

The material coordinate s is used to label the position of a cell in the original unstressed layer, and the dependent variable $x(s,t)$ describes the spatial position of a cell s at time t. In order to describe the growth of the layer, we introduce an auxiliary variable $\hat{s}(s,t)$ that describes the hypothetical (would-be) position of a cell s at time t if all deformation in the layer were instantaneously removed. Thus, $\hat{s}(s,t)$ describes the local growth of the layer at the position s. (See Figure 1.)

The introduction of $\hat{s}$ is necessary because the elastic response of the material depends on the local strain but not on growth. Material growth (and decay) of the cell layer is described using the growth gradient, g, defined as

$$g(s,t) = \frac{\partial \hat{s}(s,t)}{\partial s}. \tag{2.1}$$

The strain in the layer is defined as $\epsilon = \partial x/\partial \hat{s} - 1$, or, more formally, as

$$\epsilon(s,t) = \frac{\partial x(s,t)}{\partial s} g(s,t)^{-1} - 1. \tag{2.2}$$

(Note that $\epsilon > 0$ corresponds to stretch, and $-1 < \epsilon < 0$ corresponds to compression.)

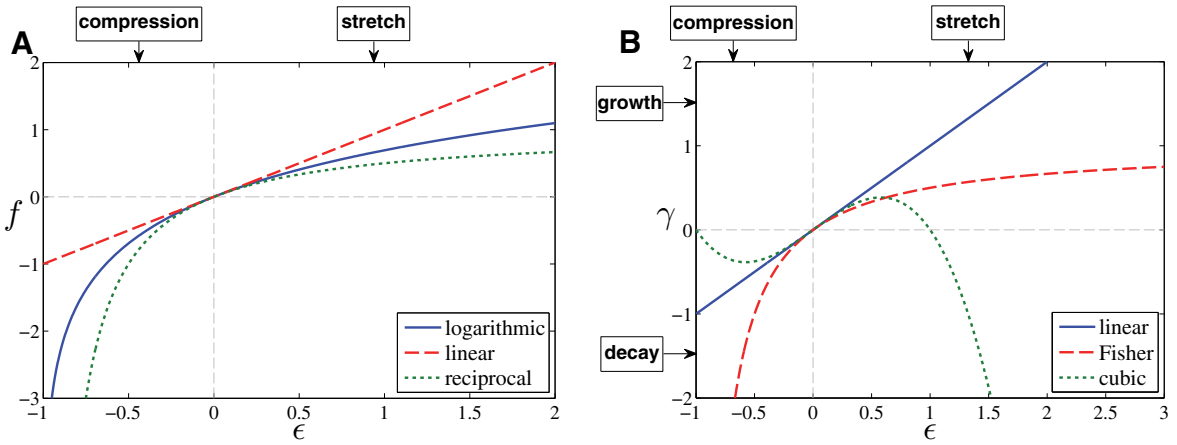

Figure 2. (A) *Resultant forces f from (2.4) that will be analyzed in this article as a function of ϵ. Here, $k = 1$. $\epsilon > 0$ corresponds to stretching of the cell layer, and $-1 < \epsilon < 0$ corresponds to compression of the cell layer.* (B) *Growth functions γ from (2.6) that will be analyzed in this article as a function of ϵ. $\epsilon > 0$ corresponds to stretching of the cell layer, and $-1 < \epsilon < 0$ corresponds to compression of the cell layer. $\gamma > 0$ corresponds to cell proliferation, and $\gamma < 0$ corresponds to cell apoptosis.*

We first discuss equations governing the elastic deformation of the layer. Mi et al. [15] derived the following governing equation for the motion of the layer:

$$b\frac{\partial x}{\partial s}\frac{\partial x}{\partial t} = \frac{\partial f}{\partial s}, \tag{2.3}$$

where b is the constant for adhesion between cells and substrate and $f(s,t)$ is the resultant force on a cross section of the layer. Here we assume that the resultant force depends explicitly on the strain via a constitutive function $\phi(\epsilon)$, i.e., that $f(s,t) = \phi(\epsilon(s,t))$. While (2.3) is a fundamental physical law, the constitutive function $\phi(\epsilon)$ describes the material under consideration and can vary from one cell layer to the next. It is natural to restrict one's attention to functions $\phi(\epsilon)$ that are monotone increasing, differentiable, and such that $\phi(0) = 0$. Examples discussed in this paper include (see Figure 2(A))

$$\text{logarithmic:} \qquad \phi(\epsilon) = k\ln(\epsilon+1), \tag{2.4a}$$

$$\text{linear (Hooke's law):} \qquad \phi(\epsilon) = k\epsilon, \tag{2.4b}$$

$$\text{reciprocal (ideal gas law):} \qquad \phi(\epsilon) = k\left(1 - \frac{1}{\epsilon+1}\right), \tag{2.4c}$$

where k is the residual stretching modulus of the cell layer after cytoskeleton relaxation. The logarithmic relation yields infinite magnitude of stress both when $\epsilon \to -1$ and when $\epsilon \to \infty$, giving an appropriate behavior at both large compressions and large extensions (Fung [10]).

The growth gradient $g(s,t)$ obeys the equation

$$\frac{\partial g}{\partial t} = \gamma g, \tag{2.5}$$

where γ is the growth rate, given by a constitutive assumption that may depend explicitly on s, t, g, and/or ϵ. In this paper we analyze the dependence of growth on stress/strain within the layer, and hence we assume that γ (like f) depends solely on ϵ. It has been observed that, for small deformations, a stretched cell layer is more likely to proliferate than a compressed layer (Bindschadler and McGrath [3]), and hence we shall assume that $\gamma(0) = 0$ and $\gamma(\epsilon) > 0$ for small positive ϵ. Examples of growth rate functions that are discussed in this article (see Figure 2(B)) include

$$\text{linear:} \quad \gamma(\epsilon) = \epsilon, \tag{2.6a}$$

$$\text{Fisher:} \quad \gamma(\epsilon) = \frac{\epsilon}{\epsilon + 1}, \tag{2.6b}$$

$$\text{cubic:} \quad \gamma(\epsilon) = -\epsilon(\epsilon^2 - 1). \tag{2.6c}$$

The set of equations (2.1)–(2.3) and (2.5) together with constitutive functions for $\phi(\epsilon)$ and $\gamma(\epsilon)$ form a complete description of the system in Lagrangian coordinates and will be called the *material formulation* of the model.

3. Numerical solutions on a finite domain. In order to obtain a better idea of the type of behavior we can expect for the cell layer migration model, we first look for numerical solutions. The material formulation of model equations is very convenient for numerical simulations since the domain of the independent variable s can be fixed. In all cases studied in this section, we assume that the cell layer has finite length and is initially uniform and free from internal stresses, and that the location of the left boundary of the cell layer (at $s = 0$) is fixed (mimicking the way cells are attached to the edge of a slide, or to a fixed structure) while the right boundary (at $s = 1$ in dimensionless units) is free to move (mimicking the edge of the wound or a gap in the layer). At the right boundary there is an applied force F, which represents the net external force that develops as a result of lamellipodia formation in cells of the epithelial layer. The traction forces generated by these lamellipodia and applied by migrating cells on the substrate arise throughout the layer, but they become strongly correlated near the moving edge [7, 26]. In this paper we are seeking traveling waves, and hence F is assumed to be constant. The full material formulation with the above specified initial and boundary conditions is

$$\frac{\partial x(s,t)}{\partial t} = \frac{1}{b}\left(\frac{\partial x(s,t)}{\partial s}\right)^{-1} \frac{\partial}{\partial s}\phi\left(\frac{1}{g(s,t)}\frac{\partial x(s,t)}{\partial s} - 1\right), \qquad 0 \le s \le 1,\ 0 \le t, \tag{3.1a}$$

$$\frac{\partial g(s,t)}{\partial t} = \gamma\left(\frac{\partial x(s,t)}{\partial s} g(s,t)^{-1} - 1\right) g(s,t), \qquad 0 \le s \le 1,\ 0 \le t, \tag{3.1b}$$

$$x(s,0) = s, \qquad 0 \le s \le 1, \tag{3.1c}$$

$$g(s,0) = 1, \qquad 0 \le s \le 1, \tag{3.1d}$$

$$x(0,t) = 0, \qquad 0 \le t, \tag{3.1e}$$

$$\phi\left(\epsilon(1,t)\right) = F, \qquad 0 < t. \tag{3.1f}$$

A numerical solution of these initial-boundary value problems (3.1) for a given growth function $\gamma(\epsilon)$, elasticity function $f = \phi(\epsilon)$, and parameters k, b, and F can be found using an

adaptive finite difference method based on the method of Mi et al. [15]. We found that using the original nonadaptive mesh results in exponential growth at the moving edge and widening of the grid spacing. By adaptively refining the mesh at positions of largest growth, we decrease numerical errors. (See Appendix A in the Supplementary Material (94140_01.pdf [local/web 970KB]) and Stepien [23] for details and analysis of the solution method.) Parameter values used were chosen based on estimates from Mi et al. [15].

Figure 3 shows the evolution of the cell layer for zero, linear (2.6a), Fisher (2.6b), and cubic (2.6c) cell proliferation functions and the logarithmic elasticity function (2.4a). See Figure B.1 in Appendix B of the Supplementary Material (94140_01.pdf [local/web 970KB]) for additional simulations.

For zero cell proliferation, we observe that the velocity of the moving edge converges to 0, and the cells move a finite distance to the right for the logarithmic and linear (2.4b) elasticity functions, as well as the reciprocal elasticity function (2.4c), although the convergence is much slower in this case. This is a limiting case of the time-dependent solution, and there is a maximum distance the right edge of the cell layer can reach, which is $\phi^{-1}(F)+1$. This phenomenon of large size wounds being unable to close was described by Mi et al. [15] and verified experimentally. The initial evolution of the finite size layer and the evolution of a layer that is semi-infinite (extending to infinity on the left-hand side) is governed by a similarity solution, which we analyze in the next section.

For the linear, Fisher, and cubic cell proliferation functions, we observe that the velocity of the moving edge converges to a positive constant, and the curves in the plots of ϵ versus $\hat{s}$ converge to a similar shape. This same behavior occurs for the logarithmic, linear, and reciprocal elasticity functions (not all results are shown here). This is indicative of a traveling wave, a wave that travels at constant velocity without change of shape. In section 5, we analyze the existence of traveling wave solutions using phase plane and bifurcation analysis.

We point out that, for the zero, linear, Fisher, and cubic growth functions, the range of the numerically realized ϵ is largest for the reciprocal elasticity function and smallest for the linear elasticity function. The nonzero growth functions behave similarly within the numerically realized ϵ ranges for the logarithmic and linear elasticity functions (see Figure 2(B)).

4. Similarity solutions for a model without growth. In cell layers of finite size, in the absence of proliferation the leading edge eventually stops moving as the stress in the layer balances the applied force at the layer's edge. In this section we show that in semi-infinite layers, however, the motion of the edge can continue indefinitely, and the solution for such cases is self-similar.

Consider the material formulation without growth ($\gamma \equiv 0$) on a semi-infinite domain $s \in (-\infty, 0]$, where the cell layer extends to infinity on the left, and the moving edge is now labeled $s = 0$. At the left boundary we replace the boundary condition (3.1e) with the limiting condition of an unstressed layer, while at the moving end we retain the condition of the applied force being equal to F. Since $\hat{s}(s,t) = s$ and $g \equiv 1$ in the absence of cell proliferation, the problem reduces as follows:

$$\frac{\partial x(s,t)}{\partial t} = \frac{1}{b}\left(\frac{\partial x(s,t)}{\partial s}\right)^{-1} \frac{\partial}{\partial s}\phi\left(\frac{\partial x(s,t)}{\partial s} - 1\right), \qquad -\infty \le s \le 0,\ 0 \le t, \tag{4.1a}$$

$$x(s,0) = s, \qquad -\infty \le s \le 0, \tag{4.1b}$$

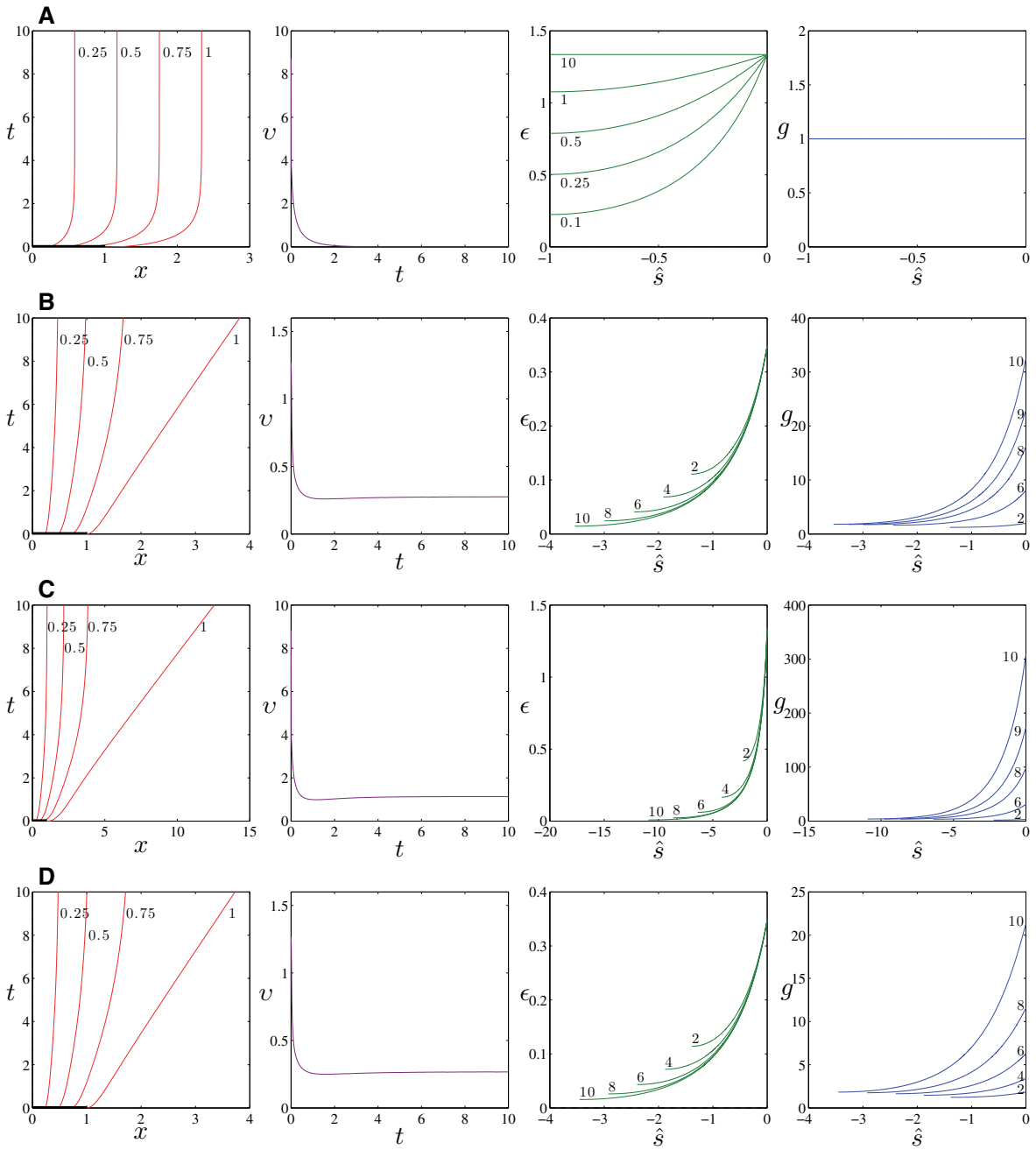

Figure 3. *Numerical solution of the model equations with the logarithmic elasticity function* (2.4a). *The first column shows the position x of cells with $s = 0.25, 0.5, 0.75, 1$ as time (in hours) increases. Each curve is labeled by its initial position between $[0, 1]$ on the x-axis and represents the path of one cell from where it begins initially to how far right it moves as time increases along the t-axis. The second column shows the velocity v of the moving edge as a function of time (in hours). The third column shows the strain ϵ as a function of position $\hat{s}$. Each curve is labeled by the time and represents the solution translated to the left so that the largest value of $\hat{s}$ for each time shown is 0. The last column shows the growth gradient g as a function of position $\hat{s}$. Each curve is labeled by the time and represents the solution translated to the left so that the largest value of $\hat{s}$ for each time shown is 0.* (A) *No growth,* $\gamma(\epsilon) = 0$, $k = 2.947$, $b = 1$, $F = 2.5$; (B) *linear growth function* (2.6a), $k = 0.838$, $b = 1$, $F = 0.25$; (C) *Fisher growth function* (2.6b), $k = 2.947$, $b = 1$, $F = 2.5$; *and* (D) *cubic growth function* (2.6c), $k = 0.838$, $b = 1$, $F = 0.25$.

$$\lim_{s\to-\infty}\frac{\partial x(s,t)}{\partial s}=1, \qquad 0\le t, \tag{4.1c}$$

$$\phi\left(\epsilon(0,t)\right)=F, \qquad 0<t, \tag{4.1d}$$

where $\epsilon(s,t)$ is as in (2.2) and $\phi(\epsilon)$ is again a constitutive function characterizing the elasticity of the layer.

We look for a similarity solution of the form

$$x(s,t)=t^{\alpha}w(z), \qquad z=t^{-\beta}s. \tag{4.2}$$

Since $\epsilon(s,t)=\frac{\partial x}{\partial s}-1=t^{\alpha-\beta}w'-1$, (4.1a) reduces to the ordinary differential equation

$$t^{\alpha-1+\beta}\left(\alpha w(z)-\beta z w'(z)\right)=\frac{1}{b}\left(w'(z)\right)^{-1}w''(z)\Phi\left(t^{\alpha-\beta}w'(z)-1\right), \tag{4.3}$$

where we define $\Phi(\epsilon)=\frac{d}{d\epsilon}\phi(\epsilon)$ and $'=\frac{d}{dz}$. The right boundary condition (4.1d) implies that $\epsilon(0,t)=t^{\alpha-\beta}w'(0)=\phi^{-1}(F)+1$. Since both $w'(0)$ and $\phi^{-1}(F)$ are constants and $w'(0)\neq 0$ by (4.1b), then $t^{\alpha-\beta}$ must be a constant and hence $\alpha=\beta$. Thus (4.3) becomes

$$\alpha t^{2\alpha-1}\Big(w(z)-zw'(z)\Big)w'(z)=\frac{1}{b}w''(z)\Phi\left(w'(z)-1\right). \tag{4.4}$$

We can make this equation t-independent for any constitutive function $\phi(\epsilon)$ if we assume one of the following relations: $w'(z)=0$, $w(z)=zw'(z)$, or $\alpha=\frac{1}{2}$. The first two relations yield only trivial self-similar solutions, since $w'(z)=0$ implies that x does not depend on s, and $w(z)=zw'(z)$ implies that x does not depend on t. Therefore, we take $\alpha=\frac{1}{2}$ and conclude that the problem (4.1) has a nontrivial similarity solution under the scaling of the form

$$x(s,t)=\sqrt{t}w(z), \qquad z=\frac{s}{\sqrt{t}}, \tag{4.5}$$

if and only if the second-order boundary value problem

$$w''(z)+\frac{b}{2\Phi\left(w'(z)-1\right)}\left(zw'(z)-w(z)\right)=0 \tag{4.6}$$

with boundary conditions (4.1c) and (4.1d) has a solution $w(z)$. Setting $y:=w'$, this becomes a system of first-order ordinary differential equations,

$$w'=y, \tag{4.7a}$$

$$y'=\frac{b}{2\Phi(y-1)}(w-zy)y, \tag{4.7b}$$

subject to the boundary conditions

$$y(0)=\phi^{-1}(F)+1, \tag{4.8a}$$

$$\lim_{z\to-\infty}y(z)=1. \tag{4.8b}$$

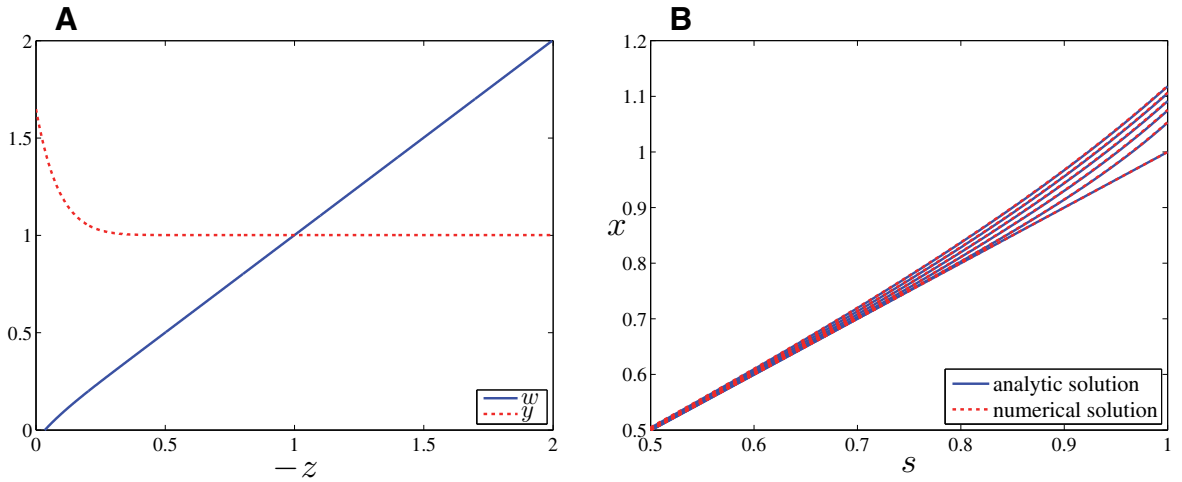

Figure 4. *Similarity solution under scaling for the material formulation with no growth, $\gamma(\epsilon) = 0$, with $k = 0.01$, $b = 1$, and $F = 0.005$.* (A) *Solution of the boundary value problem* (4.7)–(4.8) *in the z-coordinate. (Note that in this figure the direction of the z-axis is reversed, and hence the moving edge is on the left.)* (B) *The numerical solution of* (3.1)*, using an adaptive finite difference method, is plotted against the analytical solution of the boundary value problem* (4.7)–(4.8) *for $t = 0$, 1, 2, 3, 4, 5 hours.*

Our assumption that $\phi(\epsilon)$ is monotone increasing implies that the term $\Phi(y-1)$ is positive and bounded away from zero.

Figure 4(A) shows a numerical solution of (4.7)–(4.8) with logarithmic elasticity function (2.4a), solved via XPPAUT [6]. The solution shows a function $w(z)$ that decreases as z approaches the moving edge (which is on the left in Figure 4(A)), which corresponds to a stretched cell layer. Figure 4(B) shows this solution compared to the solution obtained using the adaptive finite difference method as described in section 3. Since the solution using the adaptive finite difference method is on a finite domain but the similarity under the scaling solution is on a semi-infinite domain, they match only for t that is not too large. These numerical solutions suggest that solutions of (4.7)–(4.8) exist and are unique, and future studies will focus on examining this analytically.

5. Traveling waves in a model with growth.

Experiments with cell-layer migration show that the leading edge of the cell layer moves with approximately constant velocity (Maini, McElwain, and Leavesley [14]). The same behavior is also observed in numerical simulations of the material formulation of the model shown in Figure 3(B)–(D). These observations indicate that one can expect the model to have stable traveling waves for certain types of end-conditions and that these waves should be capable of explaining some experimental observations. In this section we discuss the existence, uniqueness, and stability of traveling waves for various choices of the growth and elasticity functions. In particular, we state the conditions for existence of stationary waves (Theorem 2), show that for growth functions with a single root there is a unique traveling wave (Theorem 3), and give conditions for the existence of traveling waves for growth functions with multiple simple roots (Theorem 4). In the last case we also show that there is an upper limit on the speed of any traveling wave in the system (Proposition 5)

and that there are growth functions and boundary conditions for which a countably infinite number of traveling waves exist (Proposition 6). Finally, we use numerical simulations to analyze stability of traveling waves and show that all waves that contain interior local minima or maxima of density are unstable.

Traveling wave analysis is very difficult to do in the material (Lagrangian) formulation of the model due to the strong nonlinearity of the governing equations. Instead, we use the equivalent spatial (Eulerian) formulation of the model, which results in a nonlinear reaction-diffusion problem with a Stefan boundary condition (free boundary) replacing the fixed boundary condition at the moving edge, and new formulas for the growth functions and stress-strain relation. The material and spatial formulations are equivalent in the sense that there is a one-to-one correspondence between their solutions. Our spatial formulation is analogous to a two-dimensional spatial formulation that was first introduced by Arciero et al. [2].

While, in the material formulation as described in section 2, the primary variable is the spatial position x of each cell given as a function of the material coordinate s and the time t, in the *spatial formulation*, the state of the cell layer is described by giving the density of cells ρ as a function of the spatial coordinate x and the time t. The density function $\rho(s,t)$ of the spatial formulation is related to the position and growth functions, $x(s,t)$ and $g(s,t)$, of the material formulation as

$$\rho\left(x(s,t),t\right) = \rho_0 \left(\frac{\partial x(s,t)}{\partial s}\right)^{-1} g(s,t), \tag{5.1}$$

where ρ_0 is the density of the relaxed (stress-free) layer. A procedure for conversion between material and spatial formulations of the problem is given in Appendix C of the Supplementary Material (94140_01.pdf [local/web 970KB]). The model equation (2.3) reduces to the equation

$$\frac{\partial \rho}{\partial t} = \frac{1}{b}\frac{\partial}{\partial x}\left(\rho p'(\rho)\frac{\partial \rho}{\partial x}\right) + q(\rho), \qquad 0 \le x \le X(t),\ 0 \le t, \tag{5.2}$$

where the constitutive function $p(\rho)$ describes the density-dependent pressure within the cell layer, the growth function $q(\rho)$ describes the density-dependent net rate of change in the number of cells within the layer due to proliferation and apoptosis, and $X(t)$ is the free boundary of the domain defined to be the position of the moving edge of the cell layer in spatial coordinates (corresponding to $x(1,t)$ in material coordinates).

The spatial constitutive functions $p(\rho)$ and $q(\rho)$ are related to the material constitutive functions $f = \phi(\epsilon)$ and $\gamma(\epsilon)$, respectively, by the following conversion formulas (see Appendix C in the Supplementary Material (94140_01.pdf [local/web 970KB])):

$$\phi(\epsilon) = -p\left(\frac{\rho_0}{\epsilon+1}\right), \qquad p(\rho) = -\phi\left(\frac{\rho_0}{\rho} - 1\right), \tag{5.3a}$$

$$\gamma(\epsilon) = \frac{\epsilon+1}{\rho_0} q\left(\frac{\rho_0}{\epsilon+1}\right), \qquad q(\rho) = \rho\gamma\left(\frac{\rho_0}{\rho} - 1\right), \tag{5.3b}$$

where we require that the functions $p(\rho)$ and $q(\rho)$ obey $p(\rho_0) = q(\rho_0) = 0$, for consistency with the conditions $\phi(0) = \gamma(0) = 0$. For simplicity of exposition we assume that $p(\rho)$ is twice continuously differentiable on $(0,\infty)$, and that $q(\rho)$ is continuously differentiable and bounded

on $(0,\infty)$. Note that the monotone increasing $\phi(\epsilon)$ on $(-1,\infty)$ implies that $p'(\rho) > 0$ on $(0,\infty)$. Also note that for logarithmic constitutive equation (2.4a) we have $p(\rho) = k\ln(\rho/\rho_0)$, and hence (5.2) reduces to the classical diffusion equation

$$\frac{\partial \rho}{\partial t} = \frac{k}{b}\frac{\partial^2 \rho}{\partial x^2} + q(\rho). \tag{5.4}$$

We assume the same initial and boundary conditions as in the material formulation (see Appendix C in the Supplementary Material (94140_01.pdf [local/web 970KB])), but we examine the existence of a traveling wave on a semi-infinite domain $x \in (-\infty, X(t)]$, which has a moving boundary located at the position defined by the function $X(t)$. The full spatial formulation is

$$\frac{\partial \rho}{\partial t} = \frac{1}{b}\frac{\partial}{\partial x}\left(\rho p'(\rho)\frac{\partial \rho}{\partial x}\right) + q(\rho), \qquad x \le X(t),\ 0 \le t, \tag{5.5a}$$

$$\rho(x,0) = \rho_0, \qquad x \le X(0), \tag{5.5b}$$

$$p(\rho(X(t),t)) = -F, \qquad 0 < t, \tag{5.5c}$$

$$X'(t) = -\frac{1}{b}p'(\rho(X(t),t))\frac{\partial \rho(X(t),t)}{\partial x}, \qquad 0 < t, \tag{5.5d}$$

$$\lim_{x\to-\infty} \rho(x,t) = \rho_0, \qquad 0 \le t. \tag{5.5e}$$

Condition (5.5d) is the Stefan condition for the speed of the propagation of the free boundary (Rubinsteĭn [22]). The spatial formulation (5.5) is equivalent to a material formulation based on (3.1) in which the domain of s is taken to be the semi-infinite interval $(-\infty, 0]$ and the boundary condition (3.1e) is replaced by the limiting condition (4.1c) (as in the formulation (4.1)).

A traveling wave solution of (5.5) is a solution of the form

$$\rho(x,t) = \check{\rho}(x - ct), \tag{5.6}$$

where c is the speed of the traveling wave and the function $\check{\rho}(z)$ is defined on the interval $(-\infty, 0]$. The traveling wave represents a profile of density that moves with a constant speed c while remaining constant at any given distance from the edge, represented by the point $z = 0$. We assume that $c \ge 0$, which corresponds to the direction of motion of the edge toward the cell layer gap, i.e., in the direction of positive x. Note that, in view of the formulation (5.5), in a traveling wave the moving boundary obeys $X(t) = ct$. (For simplicity, we shall use the same notation ρ for both functions in (5.6)—it is easy to discern which function is meant by the number of arguments.) Substituting (5.6) into (5.5a), we obtain the second-order ordinary differential equation

$$\frac{d}{dz}\left(\rho p'(\rho)\frac{d\rho}{dz}\right) + cb\frac{d\rho}{dz} + bq(\rho) = 0, \tag{5.7}$$

which can be written as a system of first-order ordinary differential equations by setting

$y := d\rho/dz$:

$$\frac{d\rho}{dz} = y, \tag{5.8a}$$

$$\frac{dy}{dz} = \frac{-1}{p'(\rho)\rho}\Big((p''(\rho)\rho + p'(\rho))y^2 + cby + bq(\rho)\Big). \tag{5.8b}$$

In view of (5.6), the boundary conditions (5.5c)–(5.5e) take the form

$$\rho(0) = \rho_F, \tag{5.9a}$$

$$y(0) = y_F, \tag{5.9b}$$

$$\lim_{z\to-\infty}(\rho(z), y(z)) = (\rho_0, 0), \tag{5.9c}$$

where $\rho_F = p^{-1}(-F)$, $y_F = \frac{-cb}{p'(p^{-1}(-F))}$, and $^{-1}$ denotes the inverse function. Any solution of the boundary value problem (5.8)–(5.9) is a traveling wave solution of (5.5). Note that the condition $q(\rho_0) = 0$ implies that $(\rho_0, 0)$ is an equilibrium point of the system (5.8). Also, note that the positive value of F, which corresponds to the case in which the layer is being stretched by the force of lamellipodia, implies that the density at the moving edge is lower than the starting density; i.e., $\rho_F < \rho_0$. We will restrict the domain of the dynamical system (5.8) to $(\rho, y) \in (0, \infty) \times (-\infty, \infty)$ so that only trajectories with $\rho(z) > 0$ for $-\infty < z \le 0$ are solutions of the boundary value problem (5.8)–(5.9). This restriction is necessary in order for the solutions of the boundary value problem to correspond to physically admissible states of the system in which cell density can never be zero or negative.

It follows from our assumption about $q(\rho)$ that the limit in (5.9c) is a fixed point of the system (5.8). Therefore, a solution of the boundary value problem (5.8)–(5.9) can exist only if $(\rho_0, 0)$ is a saddle, an unstable node, or an unstable spiral. The determinant Δ and the trace τ of the Jacobian of (5.8) evaluated at $(\rho_0, 0)$ are $\Delta = \frac{bq'(\rho_0)}{p'(\rho_0)\rho_0}$ and $\tau = \frac{-cb}{p'(\rho_0)\rho_0}$. Recalling from the properties of elasticity function p that $p'(\rho) > 0$ on $(0, \infty)$, the system (5.8) has a saddle equilibrium at $(\rho_0, 0)$ if and only if $q'(\rho_0) < 0$. Furthermore, in view of our assumption that $c \ge 0$, we have $\tau \le 0$, and hence the system cannot have an unstable node or a spiral at $(\rho_0, 0)$. Let us denote by $W^u(\rho_0, 0)$ the one-dimensional unstable manifold of the saddle equilibrium $(\rho_0, 0)$. We have essentially proven the following result.

Lemma 1. *The boundary value problem (5.8)–(5.9) has a solution if and only if $q'(\rho_0) < 0$ and $(\rho_F, y_F) \in W^u(\rho_0, 0)$. The solution (if it exists) is the unique continuous segment of $W^u(\rho_0, 0)$ that extends between (ρ_F, y_F) and $(\rho_0, 0)$.*

We will be focusing our attention solely on cases in which $q'(\rho_0) < 0$. Since both $W^u(\rho_0, 0)$ and (ρ_F, y_F) depend on c, the problem of finding conditions for existence and uniqueness of traveling wave solutions of (5.5) reduces to the problem of finding conditions for existence and uniqueness of c for which $(\rho_F, y_F) \in W^u(\rho_0, 0)$. We first examine separately the existence of stationary waves, for which $c = 0$, before turning to nonstationary traveling waves.

5.1. Stationary waves. Stationary waves are solutions of (5.5) in which the density of the layer is fixed in time and depends on the spatial coordinate only. A trivial stationary wave solution for the case with $F = 0$ is $\rho(x) = \rho(z) = \rho_0$. For $F > 0$ and for nontrivial choices

of elasticity and growth functions one may be able to find stationary waves with nonconstant densities.

System (5.8) with $c = 0$ is conservative with energy

$$E(\rho, y) = \big(p'(\rho)\rho y\big)^2 - 2b\int_\rho^{\rho_0} \alpha p'(\alpha) q(\alpha)\, d\alpha, \tag{5.10}$$

and hence any solution of the system (5.8), including the unstable manifold $W^u(\rho_0, 0)$, lies on a level set of the function $E(\rho, y)$. For the existence of a stationary wave, i.e., a solution of the boundary value problem (5.8)–(5.9) with $c = 0$, it is necessary that the level set $E(\rho, y) = E(\rho_0, 0) = 0$ also contain the point $(\rho_F, 0)$. The existence result can therefore be stated as follows.

Theorem 2. *Suppose that $q(\rho)$ is continuous and bounded on $(0, \rho_0)$ with $q(\rho_0) = 0$, and differentiable at ρ_0 with $q'(\rho_0) < 0$. Let $\widehat{\rho}$ be the largest nonnegative number such that $\widehat{\rho} < \rho_0$ and*

$$\int_{\widehat{\rho}}^{\rho_0} \alpha p'(\alpha) q(\alpha)\, d\alpha = 0. \tag{5.11}$$

The boundary value problem (5.8)–(5.9) has a solution with $c = 0$ if and only if $\widehat{\rho}$ exists and $\rho_F = \widehat{\rho}$.

Proof. It is clear that the condition (5.11) with $\rho_F = \widehat{\rho}$ is necessary for the existence of the solution. It remains to be shown that $(\widehat{\rho}, 0) \in W^u(\rho_0, 0)$, i.e., that there is a connected component of the level set $E(\rho, y) = 0$ that contains both the points $(\widehat{\rho}, 0)$ and $(\rho_0, 0)$.

In view of (5.10), the definition of $\widehat{\rho}$, and the condition $q'(\rho_0) < 0$, we have that $E(\rho, 0) < 0$ for $\rho \in (0, \rho_0)$. In addition, $E(\rho, y)$ is monotone increasing in y^2 at fixed ρ. It follows that at every fixed $\rho \in (0, \rho_0)$ there are precisely two values $y^+(\rho)$ and $y^-(\rho)$ with $y^-(\rho) < 0 < y^-(\rho)$ such that $E(\rho, y^\pm(\rho)) = 0$:

$$y^\pm(\rho) = \frac{\pm 1}{p'(\rho)\rho}\sqrt{2b\int_\rho^{\rho_0} \alpha p'(\alpha) q(\alpha) d\alpha}. \tag{5.12}$$

Since $y^+(\rho)$ and $y^-(\rho)$ depend continuously on ρ (by (5.12)) and are finite (by continuity of $q(\rho)$), the points $(\widehat{\rho}, 0)$, $(\rho_0, 0)$, $\{(\rho_0, y^-(\rho)) \,|\, \rho \in (0, \rho_0)\}$, and $\{(\rho_0, y^+(\rho)) \,|\, \rho \in (0, \rho_0)\}$ all belong to a connected component of the level set $E(\rho, y) = 0$. Thus, $(\widehat{\rho}, 0) \in W^u(\rho_0, 0)$. ∎

The conditions $q'(\rho_0) < 0$ and (5.11) together imply that $q(\rho)$ must have at least two positive simple roots. One example for which (5.11) is satisfied and a stationary wave exists is when $0 < \rho_F < \rho_0$ and there exists another zero of $q(\rho)$, say ρ_1, such that $\rho_F < \rho_1 < \rho_0$, $q(\rho) > 0$ for $\rho \in (\rho_1, \rho_0)$, $q(\rho) < 0$ for $\rho \in [\rho_F, \rho_1)$, and

$$-\int_{\rho_F}^{\rho_1} \alpha p'(\alpha) q(\alpha)\, d\alpha = \int_{\rho_1}^{\rho_0} \alpha p'(\alpha) q(\alpha)\, d\alpha. \tag{5.13}$$

In such a case, the graph of $\rho p'(\rho) q(\rho)$ is of the form in Figure 5(A). Furthermore, in the phase portrait of the system, $(\rho_1, 0)$ is a center, and the direction field looks like Figure 5(B). Note that, although the density is fixed in time, the cells in the layer in this example are not

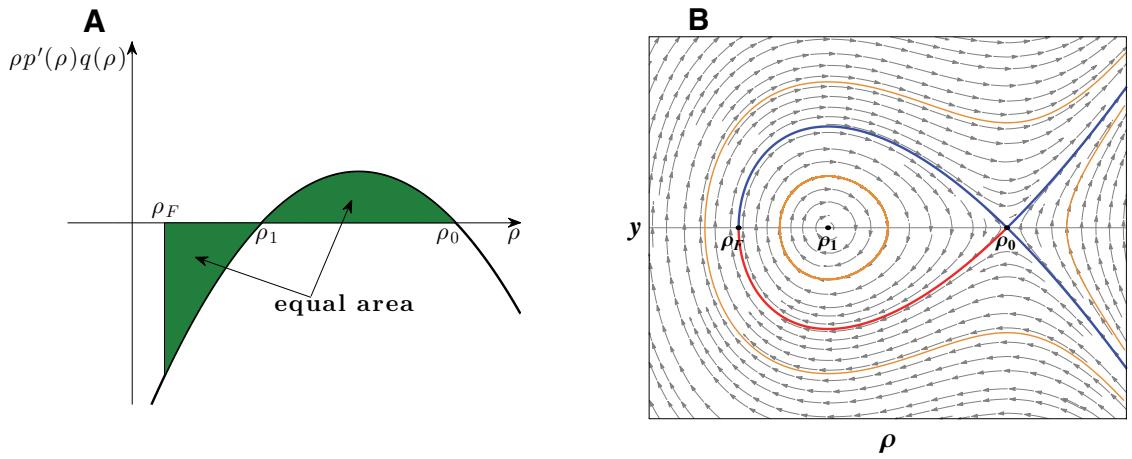

Figure 5. *Stationary wave solutions of the spatial formulation with growth.* (A) *In order to have stationary waves, the plot of* $\rho p'(\rho)q(\rho)$ *must be of this form, where there is equal area under the curve on the intervals* $[\rho_F, \rho_1]$ *and* $[\rho_1, \rho_0]$ *and the slope is positive at* ρ_1 *and negative at* ρ_0. (B) *The phase portrait for* (5.8) *with* $c = 0$ *has a center at* $(\rho_1, 0)$. *The blue lines denote the stable and unstable manifolds of the saddle point* $(\rho_0, 0)$. *The orange lines denote sample trajectories. The red line is the stationary wave solution, i.e., the portion of the unstable manifold between* $(\rho_0, 0)$ *and* $(\rho_F, 0)$.

stationary. In the portion of the layer where $\rho \in (\rho_1, \rho_0)$, the layer is growing (since $q(\rho) > 0$), while in the boundary layer where $\rho \in [\rho_F, \rho_1)$, the layer is shrinking. Thus, there is a net flux of cells from the interior towards the edge of the layer which is responsible for maintaining the constant density. This motion of cells is hidden in the spatial formulation, but it would be apparent immediately if we presented the solution in the material formulation.

5.2. Traveling waves. Traveling wave solutions of (5.5), i.e., solutions of the boundary value problem (5.8)–(5.9), may not exist for all wave speeds $c > 0$, so in this section we examine the conditions for existence and uniqueness of solutions and their dependence on the elasticity function $p(\rho)$, growth function $q(\rho)$, and the parameter F. The parameter $b > 0$ is assumed fixed. Recall that physiologically relevant elasticity functions $p(\rho)$ have root ρ_0 and are monotone increasing on $(0, \infty)$. All results that follow require that these conditions be satisfied.

In accord with Lemma 1, the solution of (5.8)–(5.9) is a segment of the unstable manifold $W^u(\rho_0, 0)$ that extends between the points (ρ_F, y_F) (representing the edge) and $(\rho_0, 0)$ (representing the infinite boundary). We find this solution by varying the wave speed c, which affects both $W^u(\rho_0, 0)$ and y_F.

Let $y^u(\bar{\rho}, c)$ be the set of all intersections of $W^u(\rho_0, 0)$ with the half-line $\{\rho = \bar{\rho},\ y \le 0\}$, i.e.,

$$y^u(\bar{\rho}, c) = \{y \le 0 \,|\, (\bar{\rho}, y) \in W^u(\rho_0, 0)\}, \tag{5.14}$$

and let $\widehat{\rho}(c)$ be the largest number such that $0 \le \widehat{\rho}(c) < \rho_0$ and $y^u(\rho, c)$ is nonempty for all $\rho \in (\widehat{\rho}(c), \rho_0)$.

The number of simple roots of growth function $q(\rho)$ and the value of F dictate how many values of c result in the solution of the boundary value problem (5.8)–(5.9). In particular, for

certain $F > 0$, if $q(\rho)$ has one root, c is unique, but if $q(\rho)$ has more than one root, c may not be unique. In this section we consider the basic choices of growth functions $q(\rho)$ and address the existence of solutions. We shall look more closely at two cases: (i) the case in which $q(\rho)$ is positive for $\rho \in (0, \rho_0)$, and (ii) the case in which $q(\rho)$ has simple roots between 0 and ρ_0. Since the force applied on the boundary corresponds to stretching force, ρ_F is always lower than ρ_0, and the behavior of $q(\rho)$ above ρ_0 will have no effect on the solutions of the boundary value problem.

We first examine the case in which $q(\rho)$ *is positive for* $0 < \rho < \rho_0$. This case represents cell layers that grow whenever the cell density drops below the stress-free density (i.e., whenever they are stretched).

Theorem 3. *Suppose that $q(\rho)$ is continuous, bounded, and positive on $(0, \rho_0)$ with $q(\rho_0) = 0$, and differentiable at ρ_0 with $q'(\rho_0) < 0$. Then for any $F > 0$ such that $\rho_F = p^{-1}(-F) \in (0, \rho_0)$ there exists a unique $c(F) > 0$ for which the boundary value problem (5.8)–(5.9) has a solution, and that solution is unique.*

Proof. Let $F > 0$ be such that $\rho_F = p^{-1}(-F) \in (0, \rho_0)$. The boundary value problem (5.8)–(5.9) has a solution for some $c \geq 0$ if there is a trajectory of (5.8) that terminates at (ρ_F, y_F) and converges to $(\rho_0, 0)$ as $z \to -\infty$, i.e., if $y_F \in y^u(\rho_F, c)$, where y^u is defined by (5.14).

We will show that (i) $\widehat{\rho}(c) = 0$, (ii) $y^u(\rho, c)$ consists of a single point for every $\rho \in (\widehat{\rho}(c), \rho_0)$, and (iii) $y^u(\rho, c)$ increases in c at fixed ρ.

For $c = 0$, $y^u(\rho_0, 0)$ consists of points from the level set $E(\rho, y) = 0$, where $E(\rho, y)$ is defined in (5.10). The eigenvector associated with the positive eigenvalue of the linearized system at $(\rho_0, 0)$ is given by

$$\begin{pmatrix} -2p'(\rho_0)\rho_0 \\ cb - \sqrt{c^2b^2 - 4bq'(\rho_0)p'(\rho_0)\rho_0} \end{pmatrix}, \tag{5.15}$$

and hence, in view of the condition $q'(\rho_0) < 0$, the slope of $W^u(\rho_0, 0)$ is positive. Thus, for $\rho < \rho_0$, $y^u(\rho, 0) = y^-(\rho)$ as defined in (5.12). Since the expression in (5.12) is single-valued, $y^u(\rho, 0)$ consists of a single point for every $\rho \in (\widehat{\rho}(0), \rho_0)$. Furthermore, in view the condition that $q(\rho) > 0$ for $\rho \in (0, \rho_0)$, the expression in (5.12) is defined for all $\rho \in (0, \rho_0)$ and hence $\widehat{\rho}(0) = 0$.

Let U_0 be the closed set in the ρy-plane bounded by the lines $\{y = 0\}$ and $\{\rho = \rho_F\}$ and the curve $\{y = y^u(\rho, 0)\}$ (see Figure 6). Consider the flow of the system with any $c > 0$. Since $q(\rho)$ is positive for $\rho \in [0, \rho_0)$, there are no other fixed points in U_0 besides $(\rho_0, 0)$. The line $\{y = 0\}$ is the ρ-nullcline, and the flow across this line is in the negative y-direction. Thus, $\{y = 0\}$ is an entrance boundary of U_0. The flow across the boundary $\{\rho = \rho_F\}$ is in the negative ρ-direction, and hence $\{\rho = \rho_F\}$ is an exit boundary of U_0. The direction field has the slope

$$\frac{dy}{d\rho} = \frac{-1}{p'(\rho)\rho}\left(\left(p''(\rho)\rho + p'(\rho)\right)y + cb + b\frac{q(\rho)}{y}\right), \tag{5.16}$$

which is decreasing in c at any fixed point (ρ, y). Hence for any $c > 0$, $\{y = y^u(\rho, 0)\}$ is an entrance boundary of U_0 across the boundary (see Figure 6). Furthermore, the slope of the

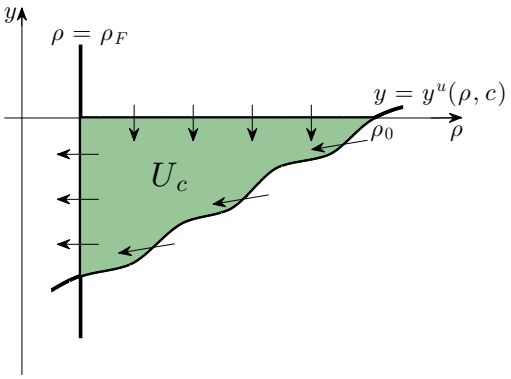

Figure 6. *The set U_c in the proof of Theorem 3 is bounded by the ρ-axis, the vertical line $\{\rho = \rho_F\}$, and the unstable manifold of the saddle $(\rho_0, 0)$, $y^u(\rho, c)$. The arrows indicate the direction of the flow with $c^* > c$.*

eigenvector associated with the positive eigenvalue of the linearized system at $(\rho_0, 0)$ decreases as c increases from 0. Therefore, for any $c > 0$, the unstable manifold $W^u(\rho_0, 0)$ enters U_0 at the point $(\rho_0, 0)$ and exits U_0 across the boundary $\{\rho = \rho_F\}$. And since $d\rho/dz < 0$ everywhere in U_0, the set $y^u(\rho, c)$ contains a unique point y for each ρ, and hence $W^u(\rho_0, 0)$ exits the set U_0 at a unique point $(\rho_F, y^u(\rho_F, c))$.

Let us now fix $c > 0$ and consider the set U_c defined in the same way as U_0 except with the boundary $\{y = y^u(\rho, 0)\}$ replaced by the boundary $\{y = y^u(\rho, c)\}$. Similarly as above, we can conclude that for each $c^* > c$ the unstable manifold $W^u(\rho_0, 0)$ exits the set U_c at a unique point $(\rho_F, y^u(\rho_F, c^*))$, where $y^u(\rho_F, c^*) > y^u(\rho_F, c)$. It follows that $y^u(\rho_F, c)$ is a continuous, monotonically increasing function of c. Recall from (5.9b) that $y_F = \frac{-cb}{p'(\rho_F)}$, and hence $y_F(c)$ continuously monotonically decreases with c such that $y_F(0) = 0 > y^u(\rho_F, 0)$ and $y_F \to -\infty$ as $c \to \infty$. By the intermediate value theorem and the monotonicity of the two functions, there exists a unique c at which $y^u(\rho_F, c) = y_F(c)$. In addition, for such c, there is a unique trajectory that terminates at (ρ_F, y_F) and converges to $(\rho_0, 0)$ as $z \to -\infty$, implying that there exists a unique solution of the boundary value problem (5.8)–(5.9). ■

The linear (2.6a) and Fisher (2.6b) growth functions are examples of growth functions that satisfy the conditions of Theorem 3. Figure 7 and the accompanying movie (94140_02.mov [local/web 1.56MB]) illustrate the phase portrait of (5.8) with a linear growth function and a logarithmic elasticity function (2.4a). Figure 8 illustrates the bifurcation diagram for this case with c as the parameter, where the line represents pairs of values of (c, F) for which a solution exists.

We now examine the case when $q(\rho)$ *has simple roots between* 0 *and* ρ_0 *and hence is both positive and negative in* $0 < \rho < \rho_0$. This case represents cell layers that grow when the cell density drops somewhat below the stress-free density, but decay (i.e., cells die off) when they are stressed too much (compressed or stretched).

Theorem 4. *Suppose that $q(\rho)$ is continuous and bounded on $(0, \rho_0)$ with $q(\rho_0) = 0$, and differentiable at ρ_0 with $q'(\rho_0) < 0$. Let $\widehat{\rho}$ be the smallest nonnegative number such that $\int_\eta^{\rho_0} \alpha p'(\alpha) q(\alpha) d\alpha \geq 0$ for $\eta \in [\widehat{\rho}, \rho_0)$. Then for any $F > 0$ such that $\rho_F = p^{-1}(-F) \in (\widehat{\rho}, \rho_0)$*

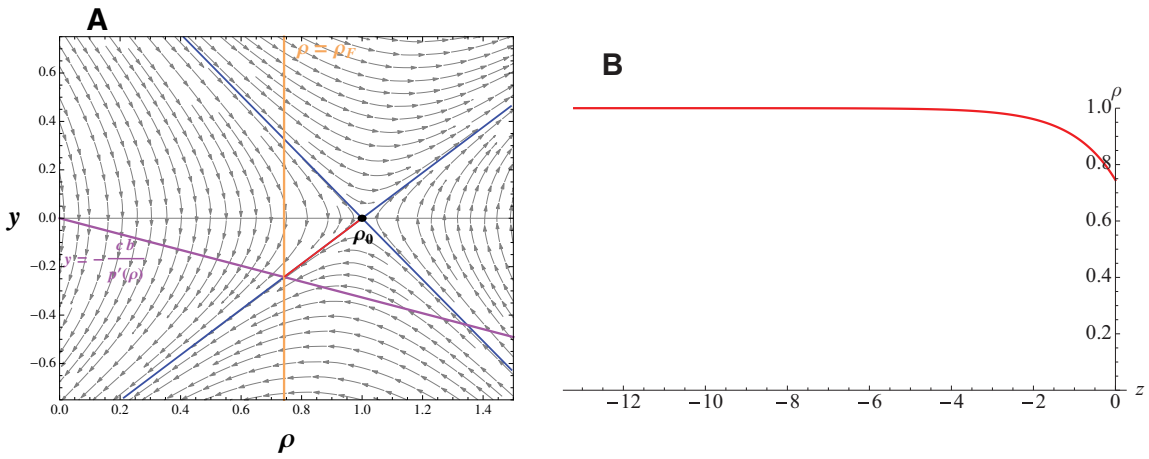

Figure 7. *Linear growth function* (2.6a) *is an example of a function that satisfies the conditions of Theorem* 3 *with logarithmic elasticity function* (2.4a). *Here,* $k = 0.838$, $b = 1$, $F = 0.25$, $\rho_0 = 1$, *and speed* $c = 0.274120$. (A) *The phase portrait of the system with the unstable and stable manifolds of the saddle point in green, the line* $\{\rho = \rho_F\}$ *in orange, the curve* $\{y = -cb/p'(\rho)\}$ *in purple, and the solution trajectory in red. The accompanying movie* (94140_02.mov [local/web 1.56MB]) *shows the phase portrait as* c *increases from* 0. (B) *The traveling wave profile of the solution trajectory in traveling wave coordinate* z; *cf. Figure* 3(B).

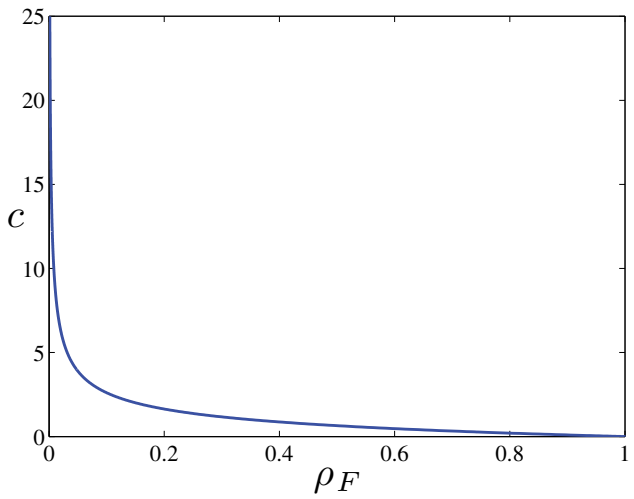

Figure 8. *The bifurcation diagram for the linear growth function* (2.6a) *with logarithmic elasticity function* (2.4a), *with parameters as in Figure* 7. *Values of* ρ_F *and* c *that lie along the curve result in unique traveling waves.*

there exists a $c(F) > 0$ *for which the boundary value problem* (5.8)–(5.9) *has a solution.*

Proof. The proof is similar to that of Theorem 3: we can construct a region analogous to U_0, except that $\{y = 0\}$ is no longer purely an entrance boundary of U_0 for the flow, and hence $W^u(\rho_0, 0)$ can exit and then re-enter U_0 across $\{y = 0\}$. If that happens, $y^u(\rho, c)$ no longer contains a single point.

Suppose that $\rho_F \in (\widehat{\rho}, \rho_0)$. In view of (5.12), $y^-(\rho_F)$ exists and is negative. Let U_0 be a closed set in the ρy-plane bounded by the lines $\{y = 0\}$, $\{\rho = \rho_F\}$, and the curve $\{y = y^u(\rho, 0)\}$. Consider the flow of the system for any $c > 0$. The line $\{\rho = \rho_F\}$ is an exit boundary of U_0, $\{y = y^u(\rho, 0)\}$ is an entrance boundary of U_0, the eigenvector of the linearized system at $(\rho_0, 0)$ decreases with c, and $d\rho/dz < 0$. Therefore, $W^u(\rho_0, 0)$ enters the set U_0 at $(\rho, 0)$ and exits the set at a point on the $\{\rho = \rho_F\}$ or $\{y = 0\}$ boundary. If $y^u(\rho_F, c)$ is nonempty, then the exit point of $W^u(\rho_0, 0)$ lies on $\{\rho = \rho_F\}$ and is given by $(\rho_F, y^u_{\min}(\rho_F, c))$, where $y^u_{\min}(\rho_F, c) = \min\{y^u(\rho_F, c)\}$. Otherwise, the exit point of $W^u(\rho_0, 0)$ lies on $\{y = 0\}$. Note that $y^u(\rho_F, 0)$ is nonempty by the assumption of the theorem.

Let us now fix $c > 0$ such that $y^u(\rho_F, c)$ is nonempty and consider the set U_c defined similarly as U_0 except with the boundary $\{y = y^u(\rho, 0)\}$ replaced by the boundary $\{y = y^u_{\min}(\rho, c)\}$. Similarly as above, we can conclude that for $c^* > c$ sufficiently small the unstable manifold $W^u(\rho_0, 0)$ exits the set U_c at a unique point $(\rho_F, y^u_{\min}(\rho_F, c^*))$, where $y^u_{\min}(\rho_F, c^*) > y^u_{\min}(\rho_F, c)$. It follows that $y^u_{\min}(\rho_F, c)$ is a continuous, monotonically increasing function of c on some interval $[0, c^\dagger]$, where $c^\dagger$ is the largest c such that $y^u(\rho_F, c)$ is nonempty. Recall from (5.9b) that $y_F = \frac{-cb}{p'(\rho_F)}$, and hence $y_F(c)$ continuously monotonically decreases with c such that $y_F(0) = 0 > y^u_{\min}(\rho_F, 0)$ and $y_F \to -\infty$ as $c \to \infty$. By the intermediate value theorem and monotonicity of the two functions, there exists a unique c at which $y^u_{\min}(\rho_F, c) = y_F(c)$. In addition, for such c, there is a unique trajectory that terminates at (ρ_F, y_F) and converges to $(\rho_0, 0)$ as $z \to -\infty$, implying that there exists a solution of the boundary value problem (5.8)–(5.9). ■

Several additional results can be obtained, as follow.

Proposition 5. *Suppose that the hypotheses of Theorem 4 are satisfied with $\widehat{\rho} > 0$. Then there exists a $c^* < \infty$ such that any solution of boundary value problem (5.8)–(5.9) with $\rho_F \in [\widehat{\rho}, \rho_0)$ has $c(F) \le c^*$.*

Proof. Let $c^* = \max_{\rho \in [\widehat{\rho}, \rho_0]} \sqrt{\frac{2}{b} \int_\rho^{\rho_0} \alpha p'(\alpha) q(\alpha) d\alpha}$. Then for $c > c^*$ the line $y = y_F(c)$ does not intersect $y^u(\rho, 0)$ at any $\rho \in (\widehat{\rho}, \rho_0)$, and since $y^u(\rho, 0) < y^u_{\min}(\rho, c)$ for all c and ρ, it follows that $y = y_F(c)$ does not intersect the set $y^u(\rho, c)$ for any $c > c^*$ and $\rho_F \in (\widehat{\rho}, \rho_0)$. Thus, in view of the proof of Theorem 4, the boundary value problem cannot have a solution with $c > c^*$. ■

Proposition 6. *Suppose that the hypotheses of Theorem 4 are satisfied with $\widehat{\rho} > 0$ and $\rho_F \in (\widehat{\rho}, \rho_0)$. The number of $c(F)$ for which the boundary value problem (5.8)–(5.9) has a solution is countably infinite.*

Proof. If $\widehat{\rho} > 0$, then the level set $E(\rho, y) = 0$ (defined in (5.10)) contains a homoclinic orbit of the system (5.8) with $c = 0$, which encloses a bounded domain U of the ρy-plane, consisting of the union of the set U_0 defined earlier and its mirror image above the ρ-axis. For any $c > 0$ the unstable manifold $W^u(\rho_0, 0)$ enters U and then remains trapped in it. By the properties of the flow, $W^u(\rho_0, 0)$ re-enters U_0 across $\{y = 0\}$ infinitely many times.

Suppose that $\rho_F \in (\widehat{\rho}, \rho_0)$. There is $c > 0$, sufficiently small, such that $W^u(\rho_0, 0)$ crosses the half-line $\{\rho = \rho_F, y < 0\}$ again at a point $(\rho_F, y^u_2(\rho_F, c))$ such that $y^u_2(\rho_F, c) \in y^u(\rho_F, c)$ and $y^u_2(\rho_F, c) > y^u_{\min}(\rho_F, c)$. In addition, $y^u_2(\rho_F, c)$ is also a continuous, monotonically increasing function of c, with $y^u_2(\rho_F, c) \to y^u(\rho_F, 0)$ as $c \to 0$, and we can repeat the last part of the above argument with $y^u_{\min}(\rho_F, c)$ replaced by $y^u_2(\rho_F, c)$ and find a (unique) value c_2 of

c such that $y_F(c_2) = y_2^u(\rho_F, c_2)$. For such c_2 the segment of $W^u(\rho_0, 0)$ between $(\rho_0, 0)$ and $(\rho_F, y_F(c_2))$ will be another solution of the boundary value problem (5.8)–(5.9). Since, in the limit $c \to 0$, the unstable manifold $W^u(\rho_0, 0)$ converges to a homoclinic orbit of (5.8) at $c = 0$, for sufficiently small $c > 0$, $W^u(\rho_0, 0)$ crosses the half-line $\{\rho = \rho_F, y < 0\}$ at $y_3^u(\rho_F, c), y_4^u(\rho_F, c), \ldots$, where $y_{j+1}^u(\rho_F, c) > y_j^u(\rho_F, c)$ for all j. By repeating the above argument, we can show that each of these additional crossings of $W^u(\rho_0, 0)$ with $\{\rho = \rho_F, y < 0\}$ will give an additional solution of the boundary value problem (5.8)–(5.9). The solutions will differ in the number of local maxima and minima of $\rho(z)$. ■

The conditions of Proposition 6 require that there be at least one other root $\rho_1 < \rho_0$ of the function $q(\rho)$ which gives rise to a stable spiral fixed point of the system. One example is the case in which the unstable manifold converges to that fixed point in the limit as $z \to \infty$. Figure 9 and the accompanying movie (94140_03.mov [local/web 4.55MB]) illustrate an example of such a situation: the phase portrait and traveling wave solution profile for the cubic growth function (2.6c), which satisfies the conditions of Theorem 4, and logarithmic elasticity function (2.4a). As c decreases, the solution trajectory winds about the spiral fixed point. For any growth function that satisfies the conditions of Theorem 4, there exists an upper bound for a countably infinite number of c in which the boundary value problem (5.8)–(5.9) has a solution. Figure 10 illustrates the bifurcation diagram, showing the values of ρ_F and c for which there is a solution to the boundary value problem, for the cubic growth function and logarithmic elasticity function.

If $\widehat{\rho} = 0$ in the statement of Theorem 4, then the number of solutions of the boundary value problem (5.8)–(5.9) is finite since ρ is the cell density and any physically relevant solution requires $\rho > 0$, and thus solution trajectories cannot traverse the loops of the stable spiral that cross the y-axis. Hence in this case, for any $\rho_F \in (0, \rho_0)$ there will be a finite number of c's for which the boundary value problem (5.8)–(5.9) has a solution. If the other fixed point of the system (see (5.13)) is nonpositive, then there will be a unique speed c, and there does not exist an upper bound on the speed c for which there is a solution. Two examples of such growth functions are $q(\rho) = (\rho_0 - \rho)(\rho_0 + 4\rho)$ and $q(\rho) = -(\rho_0 - \rho)(\rho_0 - 4\rho)$.

Let us now examine how many solutions exist for the case when $q(\rho)$ has three simple roots $0 < \rho_2 < \rho_1 < \rho_0$ or $0 < \rho_0 < \rho_1 < \rho_2$ such that, in the phase portrait, ρ_0 and ρ_2 are saddle points and ρ_1 is a stable spiral or node for sufficiently large c. An example of a phase portrait of a system with $q(\rho)$ that has roots $0 < \rho_2 < \rho_1 < \rho_0$ is illustrated in Figures 11 and 13.

If $\int_\rho^{\rho_0} \alpha p'(\alpha) q(\alpha) d\alpha > 0$ for all $\rho \in (0, \rho_0)$, as in Figure 11(A), then there exists a $c^* \in \mathbb{R}$ such that a heteroclinic orbit in the lower half of the ρy-plane connects the two saddle points ρ_0 and ρ_2 (see Figure 11(D)). There is a finite number of solutions for $\rho_F \in (0, \rho_0)$. For $c > 0$ there are a countably infinite number of solutions for $\rho_F \in (\rho_2, \eta)$ where η satisfies $\int_{\rho_2}^{\eta} \alpha p'(\alpha) q(\alpha) d\alpha = 0$. An example growth function is $q(\rho) = (\rho_0 - \rho)(\rho_0 - 2\rho)(\rho_0 - 4\rho)$, and Figure 12 illustrates the bifurcation diagram, showing the values of ρ_F and c for which there is a solution to the boundary value problem (5.8)–(5.9).

If $\int_\rho^{\rho_0} \alpha p'(\alpha) q(\alpha) d\alpha < 0$ for some $\rho \in (0, \rho_0)$, as in Figure 13(A), then the heteroclinic orbit that exists for some $c^* \in \mathbb{R}$ connecting the two saddle points ρ_0 and ρ_2 exists in the upper half of the ρy-plane (see Figure 13(D)), which cannot result in a solution assuming $c > 0$. There exists a countably infinite number of solutions for $\rho_F \in (\eta, \rho_0)$, and there exists

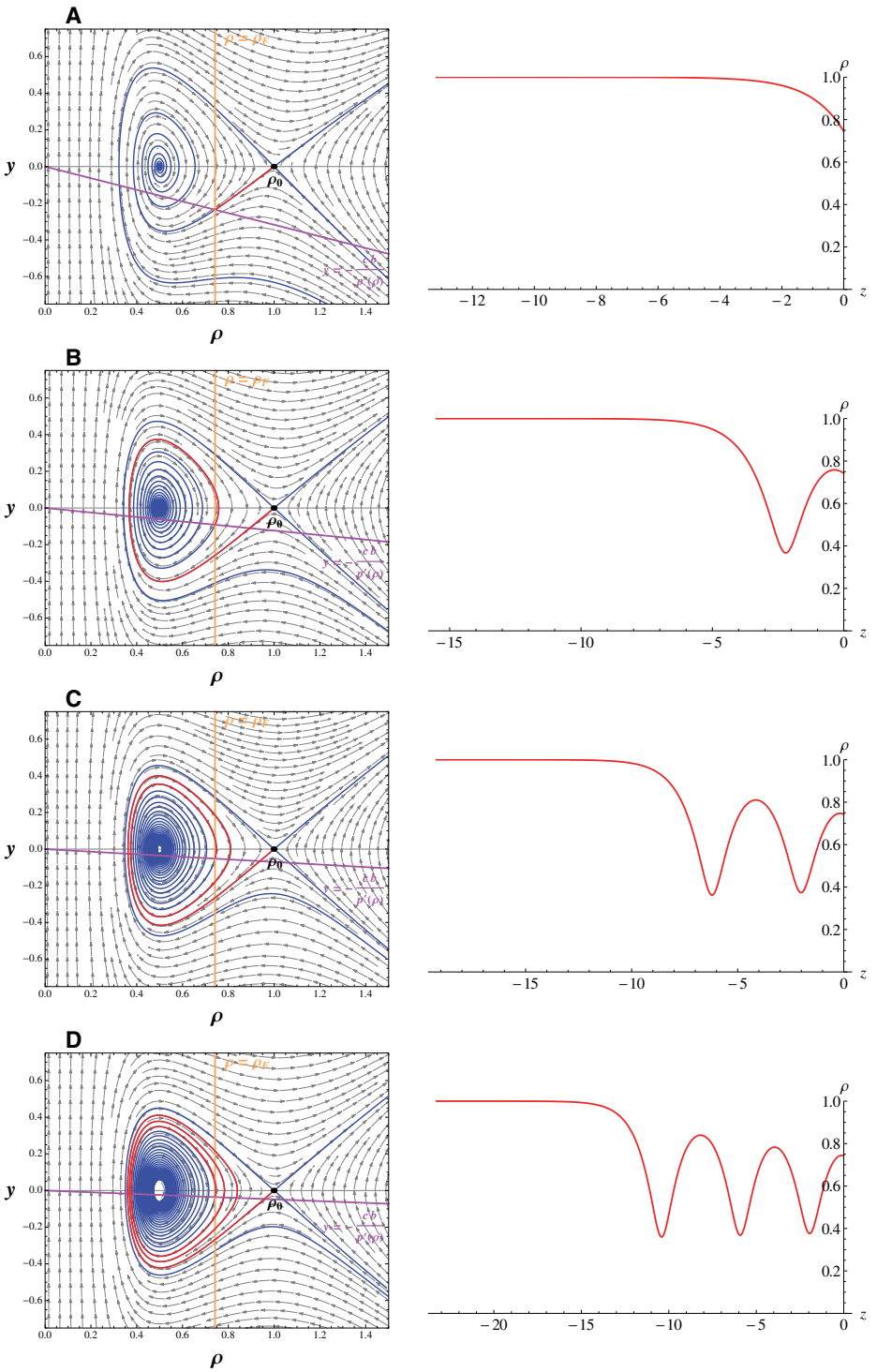

Figure 9. *Cubic growth function* (2.6c) *is an example of a function that satisfies the conditions of Theorem* 4 *with logarithmic elasticity function* (2.4a). *Here,* $k = 0.838$, $b = 1$, $F = 0.25$, $\rho_0 = 1$, *and speed is* (A) $c = 0.266062$, (B) $c = 0.103310$, (C) $c = 0.0587513$, *and* (D) $c = 0.0404030$. *First column: The phase portrait of the system with the unstable and stable manifolds of the saddle point in blue, the line* $\{\rho = \rho_F\}$ *in orange, the curve* $\{y = -cb/p'(\rho)\}$ *in purple, and the solution trajectory in red. The accompanying movie* (94140_03.mov [local/web 4.55MB]) *shows the phase portrait as* c *increases from* 0. *Second column: The corresponding traveling wave profiles of the solution trajectory in traveling wave coordinate* z; *cf. Figure* 3(D).

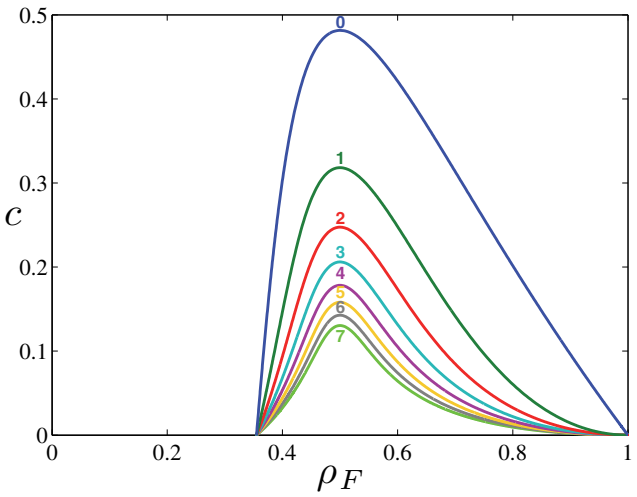

Figure 10. *The bifurcation diagram for the cubic growth function (2.6c) with logarithmic elasticity function (2.4a). Here, $\rho_0 = 1$. Values of ρ_F and c that lie along the curves result in solutions of the boundary value problem. The number of loops that the solution trajectory traverses about the stable spiral is labeled. Note that only a portion of the countably infinite number of curves is shown.*

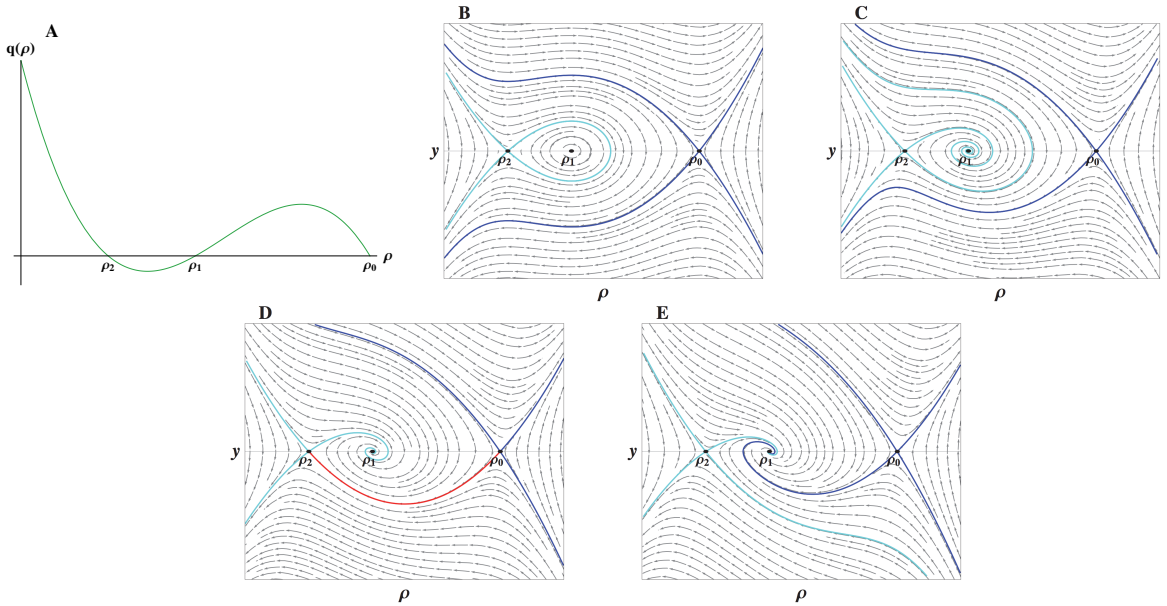

Figure 11. (A) *Growth function with three simple roots such that $\int_{\rho}^{\rho_0} \alpha p'(\alpha) q(\alpha) d\alpha > 0$ for all $\rho \in (0, \rho_0)$.* (B) *The phase portrait of the system for $c = 0$ with the unstable and stable manifolds of the saddle point $(\rho_0, 0)$ in blue and the unstable and stable manifolds of the saddle point $(\rho_2, 0)$ in cyan.* (C) *The phase portrait of the system for $0 < c < c^*$.* (D) *The phase portrait of the system for $c = c^*$. The heteroclinic orbit connecting the two saddles $(\rho_0, 0)$ and $(\rho_2, 0)$ is in red.* (E) *The phase portrait of the system for $c > c^*$.*

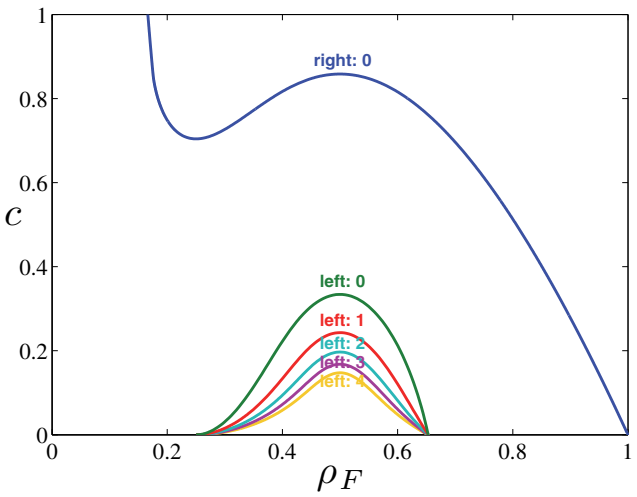

Figure 12. *The bifurcation diagram for the function* $q(\rho) = (1-\rho)(1-2\rho)(1-4\rho)$, *with logarithmic elasticity function* (2.4a). *Here, for the curve labeled "right,"* $\rho_0 = 1$, *and for the curves labeled "left,"* $\rho_0 = \frac{1}{4}$. *Values of* ρ_F *and* c *that lie along the curves result in solutions of the boundary value problem. The number of loops that the solution trajectory traverses about the stable spiral is labeled. Note that only a portion of the countably infinite number of curves is shown.*

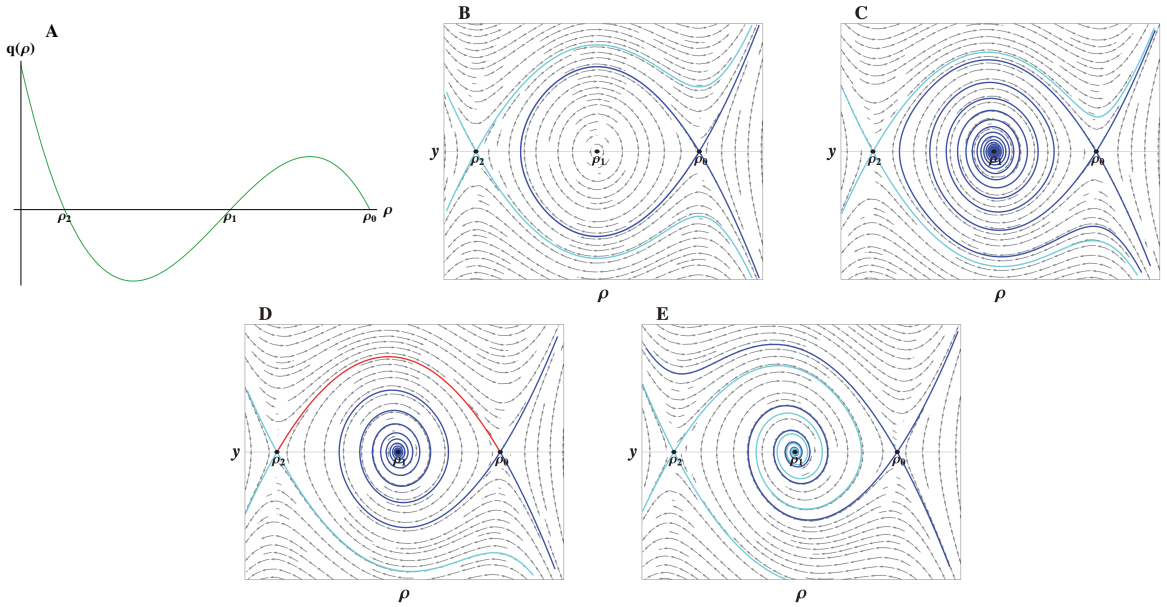

Figure 13. (A) *Growth function with three simple roots such that* $\int_{\rho}^{\rho_0} \alpha p'(\alpha) q(\alpha) d\alpha < 0$ *for some* $\rho \in (0, \rho_0)$. (B) *The phase portrait of the system for* $c = 0$ *with the unstable and stable manifolds of the saddle point* $(\rho_0, 0)$ *in blue and the unstable and stable manifolds of the saddle point* $(\rho_2, 0)$ *in cyan.* (C) *The phase portrait of the system for* $0 < c < c^*$. (D) *The phase portrait of the system for* $c = c^*$. *The heteroclinic orbit connecting the two saddles* $(\rho_0, 0)$ *and* $(\rho_2, 0)$ *is in red.* (E) *The phase portrait of the system for* $c > c^*$.

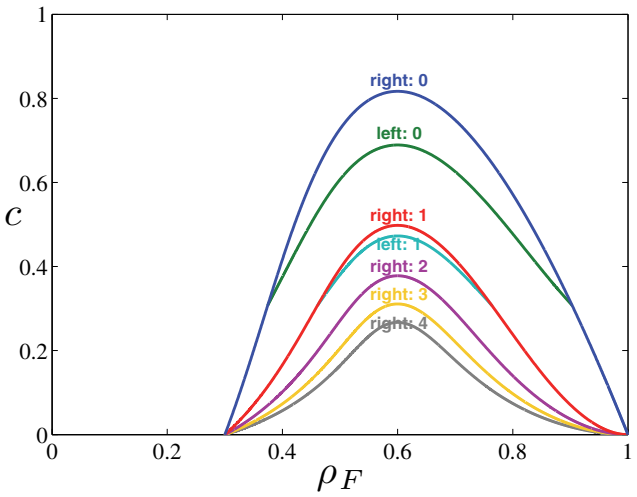

Figure 14. *The bifurcation diagram for the function* $q(\rho) = (1-\rho)(1-8\rho)(3-5\rho)$*, with logarithmic elasticity function* (2.4a)*. Here, for the curves labeled "right,"* $\rho_0 = 1$*, and for the curves labeled "left,"* $\rho_0 = \frac{1}{8}$*. Values of* ρ_F *and* c *that lie along the curves result in solutions of the boundary value problem. The number of loops that the solution trajectory traverses about the stable spiral is labeled. Note that only a portion of the countably infinite number of curves is shown.*

an upper bound on the speed c for which there is a solution. An example growth function is $q(\rho) = (\rho_0 - \rho)(\rho_0 - 8\rho)(3\rho_0 - 5\rho)$, and Figure 14 illustrates the bifurcation diagram, showing the values of ρ_F and c for which there is a solution to the boundary value problem (5.8)–(5.9).

Our analysis of the number of possible solutions of the boundary value problem (5.8)–(5.9) directly extends to the case when the growth function $q(\rho)$ has four or more simple roots. These functions will result in phase portraits with alternating saddles and stable spirals/nodes, and the number of possible solutions for a chosen ρ_F is either none, one, a finite number, or a countably infinite number. This analysis also extends to growth functions $q(\rho)$ with three or more roots with some repeated (with the exception of ρ_0, which must be a simple root). These growth functions give results similar to those for simple root functions of one lower degree.

5.3. Stability of traveling waves. Especially in those cases of the previous section where there are multiple traveling wave solutions, it is useful to analyze the stability of the traveling waves as solutions of the full partial differential equation formulation of the problem (5.5) under small perturbations. This will give insights into the physiological relevance of the solutions found in the previous section, as it is unlikely that unstable waves could be observed experimentally. We proceed to test the stability numerically, taking advantage of the fact that we have in hand a procedure for solving the material formulation of the problem numerically (recall section 3).

First, in Table 1, we compare the speed of the leading edge found numerically, as the velocity of the leading edge in the material formulation at $t = 20$, and analytically, as the speed c of the traveling wave solution in the spatial formulation, for the logarithmic elasticity function and for linear (2.6a), Fisher (2.6b), and cubic (2.6c) growth functions. The relative

Table 1

Speed of the moving edge to 6 significant digits: The velocity of the moving edge in the material formulation at $t = 20$. The analytical speed is the speed c of the traveling wave solution in the spatial formulation. For the linear and cubic growth functions, $k = 0.838$, $b = 1$, and $F = 0.25$, and for the Fisher growth function, $k = 2.947$, $b = 1$, and $F = 2.5$.

Growth function	Linear	Fisher	Cubic
Numerical speed	0.275432	1.13160	0.266753
Analytical speed	0.274120	1.12652	0.266062

error between the numerical and analytical speed estimates is less than 1% for all three growth functions.

Next, we examine whether the density profiles of the numerical solutions of the material formulation converge to the analytic traveling wave density profile of the spatial formulation. At a few equally spaced times, we calculate the density of the cell layer from the cell positions found from a numerical simulation of the material formulation via (5.1) with $\rho_0 = 1$, and discretize $\frac{\partial x}{\partial s}$ and $\frac{\partial \hat{s}}{\partial s}$ using centered difference in the interior and forward (backward) difference on the left (right) boundary. See Figure 15. The numerical density profiles converge to the analytical density profile for the linear, Fisher, and cubic growth functions with logarithmic elasticity function.

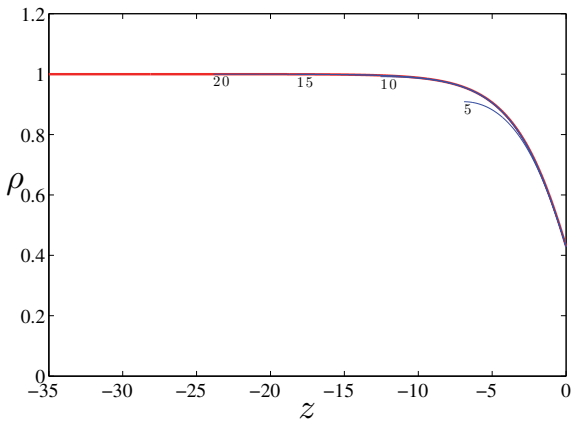

Figure 15. *Stability of traveling waves: material formulation to spatial formulation. Fisher growth function (2.6b) with logarithmic elasticity function (2.4a), $k = 2.947$, $b = 1$, $F = 2.5$, and $\rho_0 = 1$. The density profiles at $t = 5$, 10, 15, 20 hours (in blue) found numerically in the material formulation converge to the analytical traveling wave solution (in red) with $c = 1.12652$ found in the spatial formulation. Note that linear (2.6a) and cubic (2.6c) growth functions give similar convergence.*

Finally, we use the analytic traveling wave solution of the spatial formulation as an initial condition for the material formulation numerical simulations. Taking the density profile of the analytical traveling wave solution for the spatial formulation, we calculate $s = s(x, t)$ via (5.1) with $\rho_0 = 1$ and assuming $\frac{\partial \hat{s}}{\partial s} = 1$ (since $\hat{s}$ is simply a relabeling of cell positions). Thus, we numerically solve the ordinary differential equation $s' = \rho$ with initial condition $s(0) = 0$.

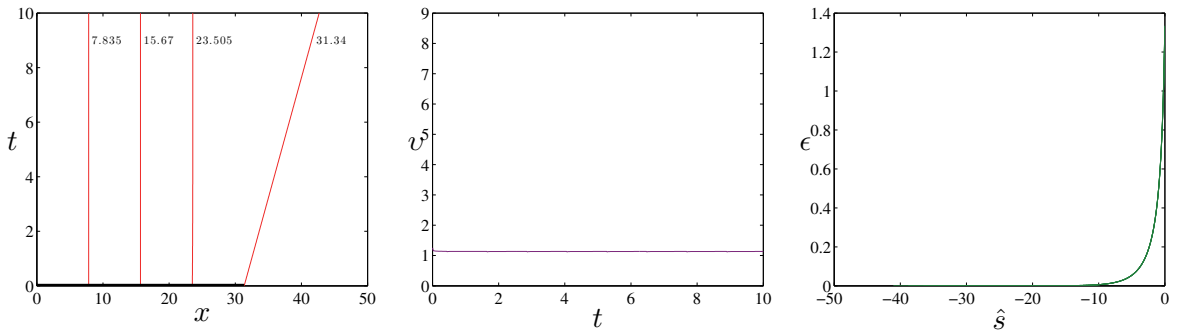

Figure 16. *Stability of traveling waves: spatial formulation to material formulation. Fisher growth function* (2.6b) *with logarithmic elasticity function* (2.4a), $k = 2.947$, $b = 1$, $F = 2.5$, *and* $\rho_0 = 1$. *The initial cell positions are found using the analytical traveling wave solution shown in Figure* 15. *Note that the linear growth function* (2.6a) *and the cubic growth function* (2.6c) *with analytical density profile shown in the second column of Figure* 9(A) *give a similar result.*

Then we must invert this solution to find $x = x(s,t)$. Using these cell positions x and s as an initial state, we find the numerical solution to the material formulation. See Figures 16–17.

For the linear and Fisher growth functions with logarithmic elasticity function, the velocity of the moving edge approximates the speeds listed in Table 1, and the shape of the plot of ϵ versus $\hat{s}$ remains unchanged throughout time, implying that the traveling wave solution persists.

For the cubic growth function with logarithmic elasticity function, we observe different behaviors based on how many loops the solution trajectory in phase space traverses about the stable spiral (cf. Figure 9). If the solution trajectory traverses no loops about the stable spiral, we observe the same behavior as for the linear and Fisher growth functions; the traveling wave solution persists. If the solution trajectory traverses one or more loops about the stable spiral, we observe that the traveling wave solution does not persist but instead converges to the traveling wave solution for the trajectory that traverses no loops. See Appendix D in the Supplementary Material (94140_01.pdf [local/web 970KB]) for additional traveling wave stability figures for the growth functions $q(\rho) = (\rho_0 - \rho)(\rho_0 - 2\rho)(\rho_0 - 4\rho)$ (see Figure D.1, which corresponds to Figures 11–12) and $q(\rho) = (\rho_0 - \rho)(\rho_0 - 8\rho)(3\rho_0 - 5\rho)$ (see Figures D.2–D.3, which correspond to Figures 13–14).

The numerical results support the following conjecture.

Conjecture. *The traveling wave solutions of the spatial formulation are stable if the solution trajectory in phase space does not cross the horizontal ρ-axis.*

6. Discussion.

We have extended the one-dimensional elastic continuum model of cell layer migration of Mi et al. [15] to include stretch-dependent proliferation, in accord with experimental observations showing that the rate of proliferation of a cell layer depends on its stretching. The material formulation of the model with no proliferation ($\gamma \equiv 0$) and linear elasticity function (2.4b), presented here, leads to the same equations as the slowly varying continuum approximation of the agent-based model of Fozard et al. [8] when neglecting internal cell viscosity. This material formulation is equivalent to the model of Arciero et al. [2] through

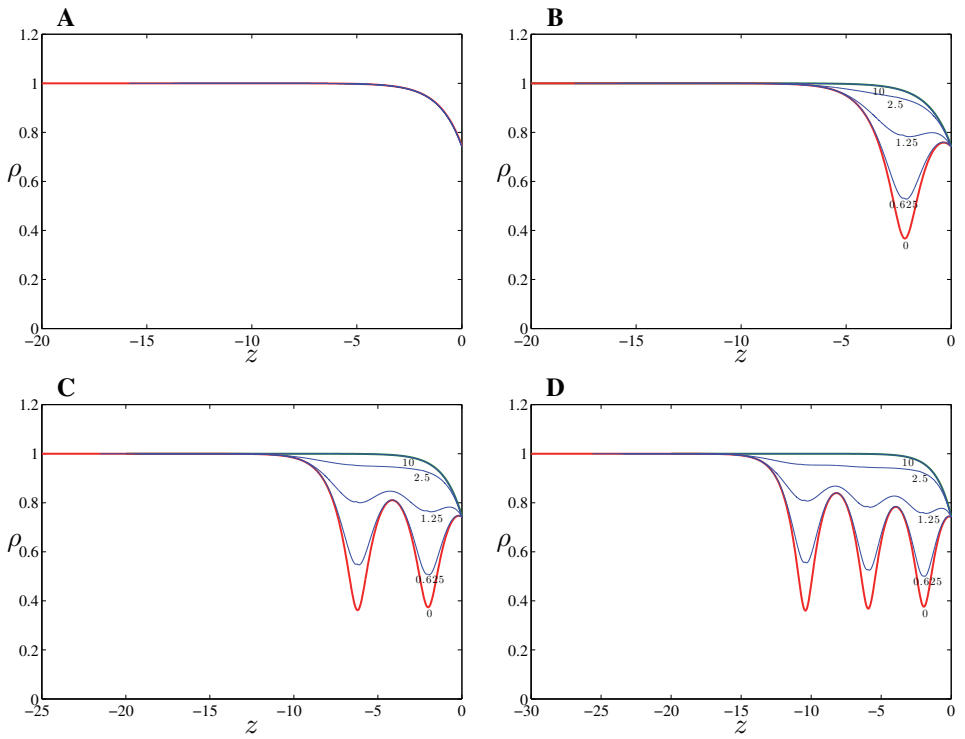

Figure 17. *Stability of traveling waves: spatial formulation to material formulation. Cubic growth function* (2.6c) *with logarithmic elasticity function* (2.4a)*,* $k = 0.838$*,* $b = 1$*,* $F = 0.25$*, and* $\rho_0 = 1$*. The initial cell positions are found using the analytical traveling wave solution shown in the second column of* (A) *Figure* 9(A)*,* (B) *Figure* 9(B)*,* (C) *Figure* 9(C)*, and* (D) *Figure* 9(D)*. For all four panels the density profiles at* $t = 0.625$*,* 1.25*,* 2.5*,* 10 *hours (in blue) found numerically in the material formulation converge to the analytical traveling wave solution (in red) shown in the second column of Figure* 9(A)*.*

point-particle interchangeability.

We solved the material formulation with stretch-dependent growth numerically using an adaptive finite difference method, which is much simpler, in terms of the number of lines of programming code, and computationally more efficient than the level set method used by Arciero et al. [2] to solve the spatial formulation. The velocity of the moving edge found in numerical simulations of the material formulation was used to determine whether traveling wave solutions might exist for certain cell proliferation rates and cell layer elasticity functions. However, analysis of the existence of traveling wave solutions was more amenable in the spatial formulation. For various nonzero cell proliferation rates and cell layer elasticity functions, we proved that traveling wave solutions with constant wave speed exist in the spatial formulation. The velocity of the moving edge found numerically approximated the analytical wave speed. Stability of the traveling wave was determined numerically; the traveling wave is stable if the corresponding trajectory in phase space does not cross the horizontal ρ-axis. For the model equations with zero proliferation, similarity solutions under scaling exist with certain conditions on the constitutive equation for elasticity.

The governing equation of the spatial formulation with logarithmic elasticity function

(2.4a) and Fisher growth (2.6b) becomes the classical Fisher–Kolmogorov equation. The typical method of proving the existence of traveling wave solutions for the Fisher–Kolmogorov equation on an infinite domain is to show the existence of a heteroclinic orbit connecting two equilibrium points, and the set of admissible traveling wave speeds for such solutions is bounded below (Murray [16]). Our model includes a Stefan condition on a moving boundary, and the traveling wave solution is solved on a semi-infinite domain instead of an infinite domain. The necessary phase space trajectory that identifies a traveling wave solution is no longer a heteroclinic orbit but a portion of an unstable manifold. We find that, in the cases described here, there is either a unique admissible traveling wave speed, a finite number of admissible traveling wave speeds, or a countably infinite number of admissible traveling wave speeds.

The majority of growth functions discussed in this article are physiologically relevant because they indicate proliferation when cells are stretched and decay when cells are compressed while the others are more theoretical in nature. Other physiologically relevant growth functions, in the material formulation, include ones of the following forms: Gaussian centered at $\epsilon = 0$ and piecewise linear approximating the Gaussian (resembling the growth rate function in Stolarska, Kim, and Othmer [24]). Our numerical simulations indicate that the leading edge of the wound eventually moves at a constant, or slowly increasing, rate for these growth functions as well; however, the proofs developed in this article do not directly apply. These functions in the spatial formulation can be considered as approximations of polynomial growth functions $q(\rho)$, and traveling wave solutions exist in a limiting sense.

In summary, our numerical and analytical results indicate that distinct constitutive equations for the cell proliferation rate and cell layer elasticity function give rise to very similar traveling wave solutions, both in shape and in speed. As a result, the inference of material properties from the shape and speed of such waves is difficult if not impossible. Most cell migration experiments tend to measure only the velocity of the wound edge and wound closure time, which data can be matched by models with various distinct constitutive equations. We suggest that the density of the cell layer should be calculated in future experiments to help elucidate the material properties, though we also hypothesize that even with this additional data the accuracy of determination of constitutive equations will not be much improved. Therefore, more data of various nature and further analysis is needed to determine accurate constitutive assumptions for the cell proliferation rate and cell layer elasticity functions for epithelial cell layer migration.

REFERENCES

[1] R. J. Anand, C. L. Leapheart, K. P. Mollen, and D. J. Hackam, *The role of the intestinal barrier in the pathogenesis of necrotizing enterocolitis*, Shock, 27 (2007), pp. 124–133.

[2] J. C. Arciero, Q. Mi, M. F. Branca, D. J. Hackam, and D. Swigon, *Continuum model of collective cell migration in wound healing and colony expansion*, Biophys. J., 100 (2011), pp. 535–543.

[3] M. Bindschadler and J. L. McGrath, *Sheet migration by wounded monolayers as an emergent property of single-cell dynamics*, J. Cell Sci., 120 (2007), pp. 1811–1821.

[4] X. Chen and A. Friedman, *A free boundary problem arising in a model of wound healing*, SIAM J. Math. Anal., 32 (2000), pp. 778–800.

[5] X. Chen and A. Friedman, *A free boundary problem for an elliptic-hyperbolic system: An application to tumor growth*, SIAM J. Math. Anal., 35 (2003), pp. 974–986.

[6] G. B. Ermentrout, *Simulating, Analyzing, and Animating Dynamical Systems: A Guide to XPPAUT for Researchers and Students*, Software Environ. Tools 14, SIAM, Philadelphia, 2002.
[7] R. Farooqui and G. Fenteany, *Multiple rows of cells behind an epithelial wound edge extend cryptic lamellipodia to collectively drive cell-sheet movement*, J. Cell Sci., 118 (2005), pp. 51–63.
[8] J. A. Fozard, H. M. Byrne, O. E. Jensen, and J. R. King, *Continuum approximations of individual-based models for epithelial monolayers*, Math. Med. Biol., 27 (2009), pp. 39–74.
[9] P. Friedl and D. Gilmour, *Collective cell migration in morphogenesis, regeneration, and cancer*, Nat. Rev. Mol. Cell Biol., 10 (2009), pp. 445–457.
[10] Y. C. Fung, *Biomechanics*, Springer, New York, 1990.
[11] E. A. Gaffney, P. K. Maini, C. D. McCaig, M. Zhao, and J. V. Forrester, *Modelling corneal epithelial wound closure in the presence of physiological electric fields via a moving boundary formalism*, IMA J. Math. Appl. Med. Biol., 16 (1999), pp. 369–393.
[12] M. Ghibaudo, A. Saez, L. Trichet, A. Xayaphoummine, J. Browaeys, P. Silberzan, A. Buguin, and B. Ladoux, *Traction forces and rigidity sensing regulate cell functions*, Soft Matter, 4 (2008), pp. 1836–1843.
[13] O. Ilina and P. Friedl, *Mechanisms of collective cell migration at a glance*, J. Cell Sci., 122 (2009), pp. 3203–3208.
[14] P. K. Maini, S. McElwain, and D. Leavesley, *Travelling waves in a wound healing assay*, Appl. Math. Lett., 17 (2004), pp. 575–580.
[15] Q. Mi, D. Swigon, B. Rivière, S. Cetin, Y. Vodovotz, and D. J. Hackam, *One-dimensional elastic continuum model of enterocyte layer migration*, Biophys. J., 93 (2007), pp. 3745–3752.
[16] J. D. Murray, *Mathematical Biology:* I: *An Introduction*, Springer, New York, 2002.
[17] S. P. Palecek, J. C. Loftus, M. H. Ginsberg, D. A. Lauffenburger, and A. F. Horwitz, *Integrin-ligand binding properties govern cell migration speed through cell-substratum adhesiveness*, Nature, 385 (1997), pp. 537–540.
[18] P. Rørth, *Collective cell migration*, Annu. Rev. Cell Dev. Biol., 25 (2009), pp. 407–429.
[19] M. P. Sheetz, D. P. Felsenfeld, and C. G. Galbraith, *Cell migration: Regulation of force on extracellular matrix-integrin complexes*, Trends Cell Biol., 8 (1998), pp. 51–54.
[20] J. A. Sherratt and J. D. Murray, *Models of epidermal wound healing*, Proc. Biol. Sci., 241 (1990), pp. 29–36.
[21] J. A. Sherratt and J. D. Murray, *Mathematical analysis of a basic model for epidermal wound healing*, J. Math. Biol., 31 (1991), pp. 703–716.
[22] L. I. Rubinsteĭn, *The Stefan Problem*, American Mathematical Society, Providence, RI, 1971.
[23] T. L. Stepien, *Collective Cell Migration in Single and Dual Cell Layers*, Ph.D. thesis, University of Pittsburgh, Pittsburgh, PA, 2013.
[24] M. A. Stolarska, Y. Kim, and H. G. Othmer, *Multi-scale models of cell and tissue dynamics*, Phil. Trans. R. Soc. A, 367 (2009), pp. 3525–2553.
[25] R. T. Tranquillo and J. D. Murray, *Mechanistic model of wound contraction*, J. Surg. Res., 55 (1993), pp. 233–247.
[26] X. Trepat, M. R. Wasserman, T. E. Angelini, E. Millet, D. A. Weitz, J. P. Butler, and J. J. Fredberg, *Physical forces during collective cell migration*, Nat. Phys., 5 (2009), pp. 426–430.
[27] P. Vitorino and T. Meyer, *Modular control of endothelial sheet migration*, Genes Dev., 22 (2008), pp. 3268–3281.
[28] C. Xue, A. Friedman, and C. K. Sen, *A mathematical model of ischemic cutaneous wounds*, Proc. Natl. Acad. Sci. USA, 106 (2009), pp. 16782–16787.